Isotherm, kinetics, process optimization and thermodynamics studies for removal of Congo red dye from aqueous solutions using *Nelumbo nucifera* (lotus) leaf adsorbent

C. Meghana[a], B. Juhi[a], Nakul Rampal[b], P. Vairavel[a,*]

[a]Department of Chemical Engineering, Manipal Institute of Technology, Manipal Academy of Higher Education, Manipal, Karnataka, India, Tel. +91 9036270978; email: pvairavel@gmail.com (P. Vairavel), Tel. +65 84307884; email: mcmchoudhary8@gmail.com (C. Meghana), Tel. +91 7587100177; email: juhibarik@gmail.com (B. Juhi)
[b]Adsorption and Advanced Materials Laboratory (AAML), Department of Chemical Engineering and Biotechnology, University of Cambridge, Philippa Fawcett Drive, Cambridge, CB3 0AS, UK, Tel. +44-737-787-5445; email: nakulrampal@gmail.com (N. Rampal)

ABSTRACT

The present study is concerned with the batch adsorption of Congo red (CR) from aqueous solutions using *Nelumbo nucifera* (lotus) leaf powder (LLP) adsorbent. Decolorization experiments were conducted in batch mode by varying experimental factors such as initial pH, adsorbate concentration, adsorbent dosage, particle size and agitation speed. The experiments are designed to attain the most optimized system using response surface methodology. The maximum adsorption efficiency is obtained at an initial pH: 6, adsorbent dosage: 6 g L^{-1}, adsorbent particle size: 42 µm and agitation speed: 150 rpm. The prepared adsorbent was characterized by proximate, particle size, Brunauer–Emmett–Teller surface area and pore volume, attenuated transmission reflector, field-emission scanning electron microscopy/energy-dispersive X-ray spectroscopy, and thermogravimetric analysis. The zero-point charge of the adsorbent was found to be at pH 6.2. The isotherm and kinetic rate constants are found using several isotherm and kinetic models, respectively. The dye adsorption rate follows a pseudo-second-order kinetic model, and the equilibrium data fit the Langmuir isotherm model with a maximum monolayer adsorption capacity (q_{max}) of 45.89 mg g^{-1} at 303 K. The adsorption mechanisms were described by pore diffusion, Bangham and Boyd plots. The overall rate of adsorption is controlled by both film and pore diffusion of dye molecules. Based on the thermodynamic analysis, the adsorption was found to be endothermic in nature, and the process was chemisorption, spontaneous and favored at high temperatures. Desorption studies were conducted with various desorbing reagents and the maximum desorption efficiency was determined using the solvent methanol. The adsorption of solute from real textile industrial CR dye effluent was carried out in batch studies using LLP adsorbent. The chemical oxygen demand removal efficiency of industrial dye effluent was 67.35%.

Keywords: Congo red dye; *Nelumbo nucifera* leaf powder; Isotherms; Thermodynamics; Kinetics; Desorption

* Corresponding author.

1. Introduction

Water pollution caused by the discharge of wastewater as a result of industrial activities has been considered one of the most serious environmental problems in the world, especially in developing countries [1]. The main sources of dye wastewater are the industries that use dyes and pigments to color their products such as textile, leather, printing, paper, plastic, ceramic, glass, food coloring, cosmetics and pharmaceutical industries [2]. The discharge of many organic and inorganic pollutants into water media from the industries mentioned above has become a global environmental problem. Currently, more than 1×10^5 dyes are commercially available having various applications with global annual production in excess of 7×10^5 million tons. Around 10%–15% of textile dyes are lost during the dyeing process and 2%–20% are directly discharged as aqueous effluent in different environmental components [3]. Among various industries, the textile industry is one of the world's most polluting industries and approximately 1,000 tons of dyestuffs are discharged into waste streams annually [4]. The release of dye effluents not only affects human health but also affects the aesthetic nature of the environment, and inhibits the photosynthetic activity in the aquatic plants by limiting sunlight penetrations and dissolved oxygen concentration. The presence of dyes in water bodies is a major cause of the increase in the value of chemical oxygen demand (COD) [5]. Most of the azo dyes have been reported to be the primary cause of lung cancer in humans, splenic sarcomas, hepatocarcinoma and chromosomal aberration in mammalian cells [6].

The synthetic dye Congo red (CR) [1-naphthalene sulfonic acid, 3,3'-(4,4'-biphenylenebis(azo))bis(4-amino-) disodium salt] is popular water-soluble diazo anionic dye, which is known to metabolize benzidine, a human carcinogen. It shows a high affinity for cellulose fibers and is used in textile processing industries. CR dye is also used in paper, printing and plastics industries to color their products. Generally, color is visible in the effluents from textile-dyeing processes when the dye concentration is greater than 1 mg L^{-1} and at an average concentration of 300 mg L^{-1} [7]. The continuous discharge of dye effluents from these industries into the receiving water bodies creates severe environmental problems since synthetic azo dyes are toxic, mutagenic, carcinogenic, and harmful to flora and fauna in water and human beings [8]. The dyes also create significant aesthetic problems as they give obnoxious color to the water [9]. CR has been known to cause allergic dermatitis, skin, eye, and gastrointestinal irritation. It is a mutagen and reproductive effector. CR dye may affect blood factors such as clotting, and induce somnolence and respiratory problems [2]. Even a low concentration of CR dye causes various harmful effects such as difficulties in breathing, diarrhea, nausea, vomiting, abdominal and chest pain, severe headache, etc. and is extremely difficult to remove due to their complex structure [10]. The effluents must be treated to bring down the concentration of dyes present in it to an acceptable and tolerable limit before releasing them into the environment [9]. Therefore, the removal of CR from effluents is of utmost importance to protect the environment and aquatic life.

Usually, conventional treatment methods such as chemical precipitation, ion exchange, membrane filtration, ion exchange, electrochemical oxidation, photo-catalytic degradation, Fenton process, ozonation, sonication, biodegradation, etc. have been widely used in the treatment of wastewater containing dyes. However, these treatment technologies have several limitations such as high capital and operating cost, sludge disposal problem, complex process, and the need for chemicals, which may thus contaminate the water [11]. The adsorption process is one of the most effective techniques for the removal of dye from the wastewater of textile and dyeing industries due to its low cost, simple and flexible design, ease of operation and insensitivity to toxic pollutants. Additionally, this process is more eco-friendly because it does not produce any harmful substances as compared to conventional treatment methods [7]. The appropriate design of the adsorption process will produce a high-quality treated effluent. Commercially available activated carbon is widely used as an adsorbent because of its excellent adsorption capacity but its use is limited due to the high cost of treatment, and difficulty in the regeneration of spent activated carbon [12]. Therefore, many researchers have studied the feasibility of using low-cost materials from agricultural by-products and plant waste materials, such as wheat bran, peanut husk, castor seed shells, cattail roots, sugarcane bagasse, and lotus leaf powder [13], etc., as adsorbents for the removal of various color from the synthetic dye effluents. These adsorbents are economically feasible and widely available in India. In addition, the regeneration of these adsorbents is not required due to availability and low-cost [3,9]. However, studies on the removal of color from CR dye from wastewater using *Nelumbo nucifera* (lotus) leaf powder (LLP) adsorbent is an area that has not been explored much. The effect of various parameters on the removal of CR from dye wastewater followed the already published papers. But not for the combination of CR dye and LLP adsorbent. To the best of our knowledge, there has practically been no work reported for describing the potential of using lotus leaf powder as adsorbent either in batch or continuous mode for the removal of CR dye from aqueous solutions. Studies need to be conducted to evaluate the use of lotus leaf powder as a low-cost adsorbent for the removal of color from wastewater. Therefore, an effort has been made to remove the color from CR dye wastewater using agricultural biomass. Response surface methodology (RSM) studies have not been performed earlier for the optimization of process parameters for the decolorization of CR dye using LLP adsorbent. Adsorption kinetics and isotherm model has to be developed in batch studies that suit the decolorization of CR from synthetic dye wastewater using lotus leaf adsorbent. In the present work, % color removal and equilibrium dye uptake of untreated lotus leaf powder as a low-cost adsorbent has been investigated, using CR as a model anionic dye. Lotus is commonly grown in subtropical and temperature regions. Lotus leaves are economically feasible and widely available natural material in India and it can easily be cultivated from seed or vegetative propagation. Its leaf contains abundant floristic fiber, protein, cellulose, hemicellulose, flavonoids, alkaloids and major functional groups (hydroxyl, methyl, alkyne, carbonyl and carboxylate) which are responsible for the adsorption of

various toxic pollutants [14,15]. The objectives of this present study are, to study the adsorption characteristics of lotus leaf powder, to analyze the effect of several process factors such as initial pH, adsorbate concentration, adsorbent dosage, adsorbent particle size and agitation speed, to optimize the various operating parameters, to determine the maximum possible adsorption capacity, to study the adsorption rate mechanism, to evaluate kinetics, isotherm and thermodynamic parameters and reusability of the adsorbent in various runs.

2. Materials and methods

2.1. Preparation of various adsorbent (agricultural by-product)

Various agricultural by-products such as rice husk, sugarcane bagasse, coir pith and sawdust were collected locally in Udupi District, Karnataka state, India. Mature *Nelumbo nucifera* leaves were collected from the Bastar district in Chhattisgarh State, India. The above materials were dried under sunlight to remove the moisture and ground to a fine powder using a pulverizer. The materials were thoroughly washed with distilled water several times to remove all the dirt particles other impurities. Then, the materials were dried in a hot-air oven at the temperature of 338 K for 8 h, ground, and screened to obtain particles <100 μm in size [16]. Various powdered materials were then stored in air-tight plastic bottles for further use in adsorption experiments.

2.2. Chemicals required

An anionic diazo acid dye CR (dye content ≥35%, molecular formula = $C_{32}H_{22}N_6Na_2O_6S_2$, molecular weight = 696.66, color index = 22120, color = brownish-red powder, λ_{max} = 498 nm) supplied by Sigma-Aldrich, India is used in the study. The dye is of analytical reagent grade, and of 99.8% purity. All other chemicals such as sodium chloride, hydrochloric acid, sodium hydroxide, methanol, ethanol, butanol, and acetone used are of analytical grade and are taken from Merck, India.

2.3. Preparation of CR dye stock solution

The required amount (1 g) of CR dye powder was dissolved in distilled water to prepare a 1,000 mg L^{-1} stock solution. The experimental solution of required initial dye concentration was obtained by diluting the stock solution with pH adjusted distilled water by adding 0.1 N HCl or 0.1 N NaOH. After dilution, the pH of the dye solution was measured and was found to be in the required range (5.6–6.4). The structure of the CR dye is shown in Fig. S1.

2.4. Analytical measurements

The pH of the dye solution was measured by a digital pH-meter (Systronics 335, India), and the average particle size of the LLP adsorbent was evaluated by a particle size analyzer (Cilas 1064, France). The surface area and pore volume of the adsorbent were determined using a Brunauer–Emmett–Teller (BET) surface analyzer (Smart Instruments, India). The residual dye concentration was estimated by measuring the absorbance at 498 nm (λ_{max}) using a pre-calibrated UV/visible spectrophotometer (Shimadzu UV-1800, Japan). Attenuated transmission reflector (ATR) spectra in the transmission range of 400–4,000 cm^{-1} was used to determine the functional groups in the LLP adsorbent and CR dye molecules loaded with adsorbent using ATR spectroscopy analysis (IR Prestige-21, Shimadzu, Japan). The surface morphology of adsorbent before and after adsorption was analyzed by field-emission scanning electron microscopy (FESEM/EDS) (CARL ZEISS-FESEM attached to Oxford instruments EDS, Germany). Analytical FESEM at 20 keV equipped with EDS was used to determine the elemental composition of the adsorbent. The thermal stability of the dried LLP adsorbent and the presence of guests, thermogravimetric analysis (TGA) (TA Instruments, England) was conducted under the following operational conditions: heating rate 283 K min^{-1}, dynamic atmosphere of argon (30 mL min^{-1}) in the temperature ranges between 323 to 1,073 K.

2.5. Adsorption experiments

The adsorption experiments were conducted at room temperature (303 K) to study the effect of various process parameters such as initial pH, initial dye concentration, adsorbent dosage, adsorbent particle size, and agitation speed on the removal of CR color from aqueous solution using LLP adsorbent. Batch experiments were performed by varying the level of one factor and keeping the level of other factors constant. Adsorption equilibrium experiments were conducted by stirring CR dye aqueous solutions at 150 rpm for 24 h with varying initial adsorbate concentration from 50 to 300 mg L^{-1} in each Erlenmeyer flask containing a fixed quantity of adsorbent dosage. A known amount of solution was withdrawn at regular time intervals. Then, the samples are centrifuged (Remi CPR-24 Plus, India) at 12,000 rpm for 10 min to separate the adsorbent from the solution [16]. After centrifugation, the clear supernatant liquid was obtained and analyzed for the residual dye concentration. The amount of CR dye adsorbed onto a unit mass of adsorbent at equilibrium and the % color removal are determined using Eqs. (1) and (2), respectively [17].

$$q_e = \frac{(C_0 - C_e)V}{W} \tag{1}$$

$$\% \text{ CR dye color removal} = \frac{(C_0 - C_e) \times 100}{C_0} \tag{2}$$

where C_0 and C_e are the initial and equilibrium adsorbate concentrations in solution (mg L^{-1}), V is the volume of dye solution (L), and W is the mass of dry LLP adsorbent (g).

2.6. Design of experiments for optimization of process parameters

The statistical design of experiments was used to obtain the overall best optimization of the process and to minimize the number of experimental trials. The RSM is a widely used as a statistical technique to design the experiments for optimization of process parameters. Various process factors were optimized using central composite design (CCD) to

attain the maximum decolorization efficiency. The factorial experimental design was used to investigate the relationship between % color removal and process factors. The experimental design was constructed through Minitab 16 statistical software and CCD was applied to conduct adsorption experiments. The influencing factors, such as initial pH (X_1), LLP adsorbent dosage (X_2), LLP adsorbent particle size (X_3) and agitation speed (X_4) were chosen as the independent variables while the % color removal was set as the response variable. The numbers of experimental runs are calculated by the following Eq. (3) [18]:

$$N = 2^f + 2f + N_0 \tag{3}$$

where f represents the number of variables, 2^f represents the number of factorial points, $2f$ represents the axial points and the center points are represented by N_0. A total of 31 experiments were conducted including 16 factorial points, 8 axial points, and 7 center points using 2^4 full factorial design. The levels of independent variables were coded as –2 (very low), –1 (low), 0 (central point), +1 (high), and +2 (very high). The coded values of process variables were obtained from Eq. (4) [19]:

$$x_i = \frac{\left(X_i - X_0\right)}{\delta X} \tag{4}$$

where x_i is the dimensionless value of a process variable; X_i is the real value of an independent variable; X_0 is the value of X_i at the center point and δX denotes the step change. The polynomial expression for the relation between the independent and response variables is given by [20]:

$$Y_p = \beta_0 + \sum \beta_i x_i + \sum \beta_{ii} x_i^2 + \sum \beta_{ij} x_i \tag{5}$$

where Y_p is the predicted response variable of % color removal; β_0 is the offset term (intercept value); and β_i, β_{ii}, and β_{ij} are the regression coefficients for linear, quadratic, and interaction effects, respectively. The sign of each coefficient suggests the direction of the relationship with response variable. The experimental ranges and levels of various independent variables in CR color removal are given in Table 1.

2.6.1. Residual analysis

To verify the predicted data obtained from RSM, the predicted responses were compared to the experimental values.

The root mean square error (RMSE) and the absolute average deviation (AAD) are used to predict the adequate precision of the model equation. The RMSE and AAD were determined using the following Eqs. (6) and (7), respectively [16].

$$RMSE = \sqrt{\left(\frac{1}{N}\sum\left(Y_a - Y_p\right)^2\right)} \tag{6}$$

$$AAD = \frac{1}{N}\sum\left(\frac{Y_p - Y_a}{Y_a}\right) \times 100 \tag{7}$$

where Y_a is the actual response value, Y_p is the predicted response value obtained from the RSM, and N is the number of experiments.

2.7. Adsorption equilibrium isotherm models

The adsorption isotherms are essential for the description of the adsorption process. It expresses the equilibrium relationship between the amount of solute adsorbed on the adsorbent (mg g⁻¹) and the adsorbate concentration remaining in the solution (mg L⁻¹) at a constant temperature. In this study, Freundlich, Langmuir and Temkin isotherms models were applied to the equilibrium data of adsorption. The applicability and suitability of the model to the equilibrium data were measured by analyzing the values of the correlation coefficients, R^2, chi-square error, χ^2 and q_e. The Freundlich isotherm model suggests that the stronger binding sites are occupied first and the adsorption binding strength decreases with increasing degree of site occupation. The linear form of the Freundlich model is given as in Eq. (8) [21].

$$\log q_e = \log K_F + \frac{1}{n}\log C_e \tag{8}$$

where K_F and $1/n$ are the Freundlich constant (L g⁻¹) and heterogeneity factor, respectively, which indicate the capacity and intensity of adsorption. The Langmuir model assumes that the adsorbed layer is the unimolecular and equal distribution of binding energy onto the solid particle surface without the transmigration of adsorbate over the surface. According to this isotherm, an active binding site becomes inactive once a dye molecule is adsorbed onto it. The linear form of the Langmuir isotherm model is given by [22]:

$$\frac{1}{q_e} = \frac{1}{q_{\max}} + \frac{1}{q_{\max} K_L C_e} \tag{9}$$

Table 1
Experimental range and levels of independent variables for CR dye removal by LLP adsorbent

Independent variables	Range and level				
	–2	–1	0	1	2
Initial pH (X_1)	5.6	5.8	6.0	6.2	6.4
LLP adsorbent dosage, g L⁻¹ (X_2)	2.0	4.0	6.0	8.0	10.0
LLP adsorbent particle size, μm (X_3)	42	68	94	120	146
Agitation speed, rpm (X_4)	80	115	150	185	220

where K_L is the Langmuir constant (L mg^{-1}) and q_m is the maximum monolayer saturation capacity of the adsorbent (mg g^{-1}). The essential characteristic of the Langmuir isotherm can be expressed by the dimensionless constant called equilibrium parameter, R_L which is defined by the following Eq. (10) [23]:

$$R_L = \frac{1}{1 + K_L C_0} \qquad (10)$$

The value of R_L indicates the type of isotherm to be either irreversible ($R_L = 0$), favourable ($0 < R_L < 1$), linear ($R_L = 1$) or unfavorable ($R_L > 1$) [7]. The Temkin isotherm is based on the assumption that the heat of adsorption decreases linearly as adsorbate-adsorbent interactions increase, and adsorption is characterized by a uniform distribution of maximum binding energy. It is given by the following linear Eq. (11) [24]:

$$q_e = \frac{RT}{b_T} \ln K_T + \frac{RT}{b_T} \ln C_e \qquad (11)$$

where K_T is the Temkin isotherm constant (L g^{-1}), RT/b_T indicates the heat of adsorption, b_T is the adsorption energy (kJ mol^{-1}), and T and R are the absolute temperature (K) and the universal gas constant (J mol^{-1} K^{-1}), respectively.

2.7.1. Error analysis of isotherm models

To determine the best isotherm model for adsorption of CR onto LLP adsorbent, the chi-square (χ^2) error analysis was carried out using the experimental data. If the predicted data from the isotherm model are similar to the experimental value, χ^2 will be a small number; if they are different, χ^2 will be a large number. The χ^2 value was calculated using the following Eq. (12) [25]:

$$\chi^2 = \sum \left[\frac{\left(q_{e,\text{expt.}} - q_{e,\text{pred.}} \right)^2}{q_{e,\text{pred.}}} \right] \qquad (12)$$

where $q_{e,\text{expt.}}$ and $q_{e,\text{pred.}}$ are the experimental and predicted adsorption capacity of CR (mg g^{-1}) at equilibrium, respectively.

2.8. Thermodynamic parameters

The thermodynamic parameters were obtained by the adsorption of CR in the temperature range from 303 to 323 K. The adsorption thermodynamics is essential to investigate whether the process is spontaneous or not and also to determine the nature of the adsorption process. The thermodynamic parameters, such as a change in Gibbs free energy (ΔG), enthalpy (ΔH), and entropy (ΔS) of the process for the adsorption of CR dye were computed using the following Eqs. (13) and (14) from the adsorption equilibrium constant, K_a (L g^{-1}) ($K_a = q_{\max} K_L$) [26]:

$$\Delta G = -RT \ln \left(K_a \right) \qquad (13)$$

$$\ln K_a = \frac{\Delta S_{\text{ads}}}{R} - \frac{\Delta H_{\text{ads}}}{RT} \qquad (14)$$

The activation energy (E_a) for the adsorption of CR onto adsorbent was determined using the Arrhenius equation. The linear form of the Arrhenius Eq. (15) is expressed as [26]:

$$\ln K_2 = \ln A - \left(\frac{E_a}{RT} \right) \qquad (15)$$

where A is the Arrhenius frequency factor, and K_2 is the rate constant of pseudo-second-order adsorption (g mg^{-1} min^{-1}). The value of K_2 is obtained from each of the reactions performed at various temperatures with different concentrations of dye solutions. The type of adsorption phenomena is generally classified as either physical or chemical based on the values of activation energy and enthalpy change [7].

2.9. Adsorption kinetic models

A study of the kinetics of adsorption is desirable as it provides information about the rate-controlling step and mechanism of adsorption, which is important to determine the efficiency of the process. The prediction of batch adsorption kinetics is necessary for the design of industrial adsorption columns and to develop mathematical models to describe the process. The Lagergren pseudo-first-order and Ho's second-order kinetic models are commonly used to fit the experimental data to determine the kinetic constants. The mathematical representations of these two models are given in Eqs. (16) and (17), respectively [27,28].

Lagergren pseudo-first-order kinetic model:

$$\ln \left(q_e - q_t \right) = \ln q_e - K_1 t \qquad (16)$$

where q_e and q_t are the adsorption capacity of adsorbent (mg g^{-1}) at equilibrium and at time t, respectively, K_1 is the rate constant of the pseudo-first-order adsorption (min^{-1}).

Ho's pseudo-second-order kinetic model:

$$\frac{t}{q_t} = \frac{1}{K_2 q_e^2} + \frac{t}{q_e} \qquad (17)$$

The initial rate of adsorption, h (mg g^{-1} min^{-1}) is given by the Eq. (18) [26]:

$$h = K_2 q_e^2 \qquad (18)$$

The mechanism of adsorption is explained by the intraparticle diffusion (pore diffusion) model and it is described by the Eq. (19) [29]:

$$q_t = K_i t^{0.5} + C \qquad (19)$$

where K_i is the intraparticle diffusion rate constant (mg g^{-1} min$^{-1/2}$) and C is the constant. The Boyd and Bangham kinetic expressions are used to predict the rate-determining step in the adsorption process. These two kinetic expressions are described by the following Eqs. (20) and (22) [26,30]:

Boyd kinetic expression:

$$F = 1 - (6 / \pi^2) \exp \left(-B_t \right) \qquad (20)$$

$$F = \frac{q_t}{q_e} \qquad (21)$$

where F is the ratio of solute adsorbed on the adsorbent at any time t to equilibrium, and B_t is a mathematical function of F.

Bangham kinetic expression:

$$\log\left(\log\left(\frac{C_0}{(C_0 - q_t m)}\right)\right) = \log\left(\frac{k_0 m}{2.303 V}\right) + \alpha \log t \qquad (22)$$

where m is the mass of LLP adsorbent used per volume of solution (g L^{-1}), α is a constant and k_0 is the Banghams constant (L^2 g^{-1}).

2.10. Validity of kinetic models

The adsorption kinetics of CR onto the prepared LLP adsorbent was verified at different initial dye concentrations. The validity of the kinetic model is evaluated using the normalized standard deviation (SD, %), given by the following Eq. (23) [31]:

$$SD(\%) = \sqrt{\sum\left[\frac{\left[\frac{(q_{e,\text{expt.}} - q_{e,\text{pred.}})}{q_{e,\text{expt.}}}\right]^2}{N_p - 1}\right]} \times 100 \qquad (23)$$

where N_p is the number of data points.

2.11. Desorption studies and reusability of the adsorbent

Desorption experiments are conducted using various desorbing reagents, such as methanol, ethanol, butanol, acetone, and 1 M NaOH in separate batches to explore the possibility of recovery of adsorbent [7,26]. In a typical desorption experiment, 100 mL of the above-mentioned desorbing reagents are added to the adsorbent loaded with adsorbed CR dye molecules and the solution is agitated at 150 rpm for 24 h in separate batches. A 100 mL of methanol is added to various conical flasks containing 0.729, 0.634, and 0.528 g adsorbent loaded with adsorbed CR dye molecules in the first, second and third run, respectively and the solution is agitated for 24 h in all three runs to desorb the dye molecules. The process was continued till the dye has been desorbed by the desorbing reagent, following which the centrifugation process was used to separate the regenerated adsorbent and desorbed dye molecules. In order to establish the reusability of the adsorbent, consecutive adsorption-desorption cycles were repeated (three times) by using the same adsorbent. The desorption for the second and third runs was carried out with 100 mL of the above-mentioned variety of desorbing reagents in separate batches. The regenerated adsorbent after desorption was collected by centrifugation and was left to dry at 338 K for 8 h. The decolorization efficiency of the regenerated adsorbent was tested in second and third runs under the optimized values of the process factors and compared with the first run. The efficiency of desorbed dye from the adsorbent was calculated using the following Eq. (24) [12]:

$$\text{Desorption efficiency} = \frac{\text{Concentration of CR dye desorbed}}{\text{Concentration of CR dye adsorbed}} \times 100 \qquad (24)$$

3. Results and discussions

3.1. Selection of suitable agricultural by-product

Adsorption experiments were performed using various agricultural by-products such as *Nelumbo nucifera* leaf, rice husk, sugarcane bagasse, coir pith and sawdust powder at room temperature to evaluate the maximum % of CR color removal and the results were shown in Fig. S2. It shows that the maximum decolorization efficiency of CR was observed in the adsorbent *Nelumbo nucifera* leaf powder. The maximum color removal using LLP adsorbent was 85.24% at pH 6 and at 8 h. It may be due to the availability of more number of active sites in the LLP adsorbent surface. Therefore, out of five different adsorbent options, *Nelumbo nucifera* leaf powder was found to exhibit better results and hence was studied for further analysis.

3.2. Characterization of the LLP adsorbent

The BET surface area and pore volume of the adsorbent were found to be 4.72 m^2 g^{-1}, 7.1 mm^3 g^{-1}, respectively, with the average particle size of 93.80 μm. The physical characteristics of the LLP were determined, and the results are reported in Table S1. It shows that a lower % of moisture (10.34%) and ash content (7.38%) signifies the better quality of the adsorbent [32]. ATR spectra of the adsorbent before and after CR dye adsorption are shown in Fig. 1. The ATR spectrum of the adsorbent before adsorption shows a broad and strong peak at 3,297 cm^{-1}, representing the O–H stretching of bonded hydroxyl groups. The narrow and strong peak at 2,940 cm^{-1} is attributed to the C–H bending vibrations of methyl groups. The peak observed at 2,352 cm^{-1} is due to O=C=O stretching of the alkyne group. The presence of C=O stretching vibrations of carbonyl groups of carboxylic acid, aromatic aldehyde and ketones with intermolecular hydrogen bond is observed from the peak at 1,619 cm^{-1}. The stretching vibration of carboxylate ion is detected by the peak at 1,285 cm^{-1}. Similarly, the bending vibrations of –OH and stretching vibrations of C–O–C were observed in the form of the peak at 1,029 cm^{-1}. A short peak at 486 cm^{-1} corresponds to =C–H bending vibrations of alkynes. After adsorption, significant changes have been observed in band intensities of hydroxyl (3,262 cm^{-1}), methyl (2,885 cm^{-1}), alkyne (2,341 cm^{-1}), carbonyl (1,630 cm^{-1}) and carboxylate (1,308 cm^{-1}) groups in the ATR spectra of CR-loaded with LLP adsorbent. Thus, the ATR spectral analysis results demonstrate that these above-mentioned functional groups may act as possible binding sites for CR molecules due to strong electrostatic interactions. A frequency shift was

observed for all band positions after CR dye adsorption [33]. Scanning electron microscopy images of the adsorbent before and after adsorption of CR dye are shown in Figs. 2a and b, respectively. As seen in Fig. 2a, adsorbent has a rough fibrous morphology. The rough surfaces are favorable for the adsorption of CR dye molecules onto the adsorbent [7]. The presence of dye molecules loaded onto the surface of the adsorbent after adsorption is shown in Fig. 2b. The chemical characteristics of the surface of the LLP adsorbent are given in Table S2. It shows that the adsorbent surface mainly contains the elements of carbon and oxygen. After
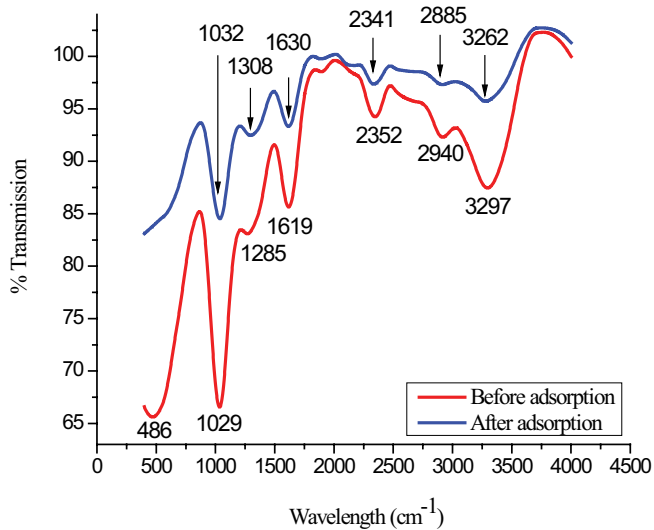
adsorption the weight and atomic % of elemental carbon and oxygen increase, suggesting that the particle surface is loaded with dye anions. TGA results are shown in Fig. 3. It shows that weight loss consists of three distinct steps in the curves. The first stage at the temperature range of (323–363 K) corresponds to a rapid loss of about 3.82% of the sample weight due to non-dissociative physically absorbed water molecules as well as water held on the surface by hydrogen bonding. The weight % loss at this temperature is due to the elimination of water molecules. The second weight loss at the temperature range of 513–723 K is 53.17%. This may be attributed to the degradation of cellulose/hemicellulose and lignin. In the temperature range (743–903 K) there is a third weight loss of 27.64%, which is corresponding to a reduction in carbonaceous residues.

3.3. Analysis of batch adsorption studies

3.3.1. Effect of initial pH

Adsorption of the CR dye by the LLP adsorbent is affected by the pH of the dye solution and the zero-point charge (pH_{zpc}) of the adsorbent. The pH point of zero charge of the adsorbent was determined by the powder addition method [34]. The ΔpH ($pH_{initial} - pH_{final}$) for the LLP adsorbent is plotted against the initial pH values. (Fig. 4). The pH_{zpc} is the initial pH at which ΔpH becomes 0 and has been found to occur when the pH reaches 6.2. The presence of H^+ and OH^- ions in solution may change the potential surface charges of the adsorbent. If the pH of the solution is below the pH_{zpc}, the binding sites on the surface will be protonated by the presence of excess H^+ ions and are positively charged. The adsorbent is negatively charged if the pH of the solution is above pH_{zpc}. This is because the active sites will be

Fig. 1. ATR spectrum of LLP adsorbent before and after CR dye adsorption.
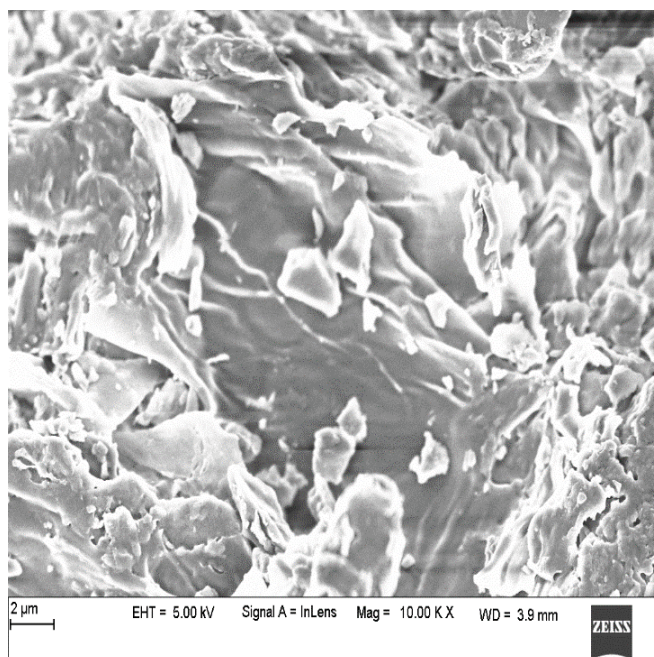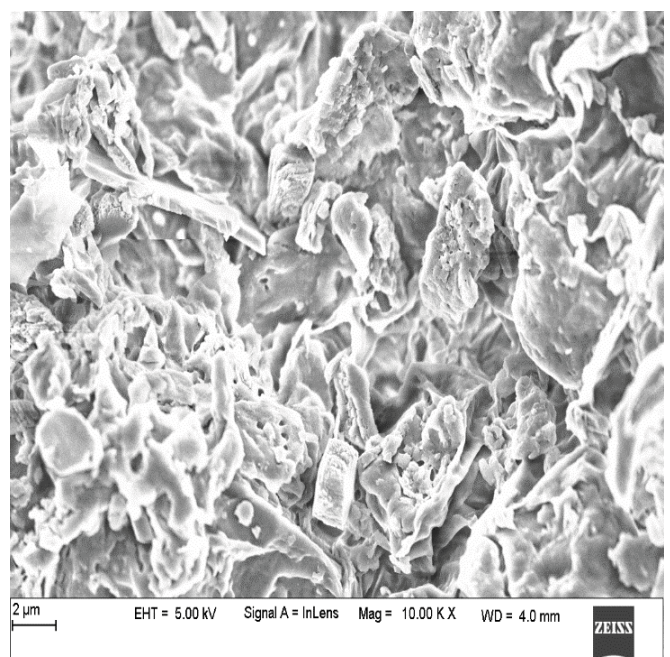
Fig. 2. Scanning electron microscopy micrograph of LLP adsorbent (a) before CR dye adsorption and (b) after CR dye adsorption.

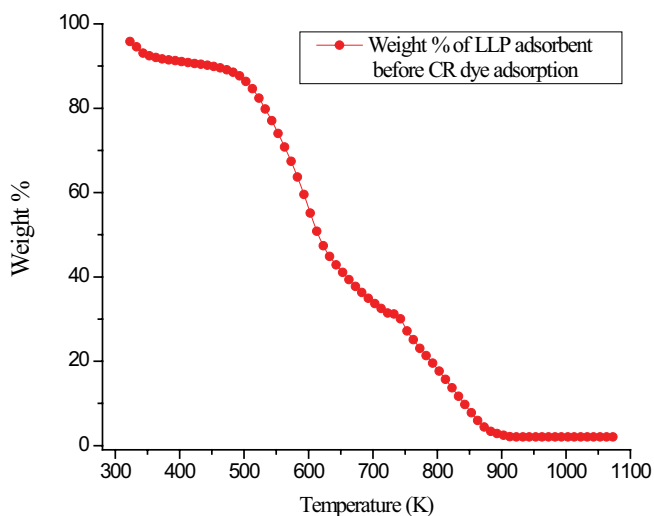Fig. 3. TGA curve of LLP adsorbent before CR dye adsorption.

Fig. 4. Zero-point charge (pH$_{zpc}$) plot of LLP adsorbent. (Sodium chloride concentration: 0.1 M; LLP adsorbent dosage: 10 g L^{-1}; LLP adsorbent particle size: 93.80 μm; agitation speed: 150 rpm; temperature: 303 K; contact time 24 h).

deprotonated by the OH$^-$ ions present in the solution. Anion adsorption on any adsorbent will be favorable at pH < pH$_{zpc}$. To analyze the effect of the initial pH on CR dye decolorization under a strongly acidic pH is difficult because of the formation of protonated species, which may lead to a change in the structure of the dye. The CR dye in aqueous solution was black in color at acidic pH (<5), due to the formation of a quinonoid structure. The red color remained stable in the pH range of 6–12, and it becomes unstable if the solution pH decreases below 5.5. The color of CR in aqueous solutions is strongly pH-dependent due to its structural transformation [35]. Therefore, the effect of initial pH on the adsorption of CR from aqueous solution was analyzed between pH 6–12. As shown in Fig. S3, the decolorization efficiency of CR decreased from 78.34% to 12.84% when the solution pH increased from 6 to 12. This phenomenon could be due to the increase in the repulsive forces between the functional groups present on the surface of the adsorbent and the CR dye molecules. As the pH of the solution increases, the active sites on the surface of the adsorbent will be deprotonated by the presence of excess OH$^-$ ions, hence resulting in the number of negatively-charged sites increasing. A negatively-charged surface site on the adsorbent does not favor the adsorption of the CR dye anions due to electrostatic repulsion. The maximum % adsorption of CR was observed at pH 6. At pH 6, a significant electrostatic attraction exists between the protonated binding sites of the adsorbent and anionic dye molecules along with van der Waals forces. Also, lower % adsorption of CR observed at basic pH is also due to competition between the excess hydroxyl ions and the negatively charged dye ions for the adsorption active sites [26]. Therefore, the possible mechanisms of CR dye adsorption may be electrostatic interactions between protonated adsorption sites of the adsorbent and negatively charged dye anions in addition to hydrogen bonding forces [10].

3.3.2. Effect of LLP adsorbent dosage

Adsorbent dosage is another important parameter for the determination of the adsorption capacity. The effect of
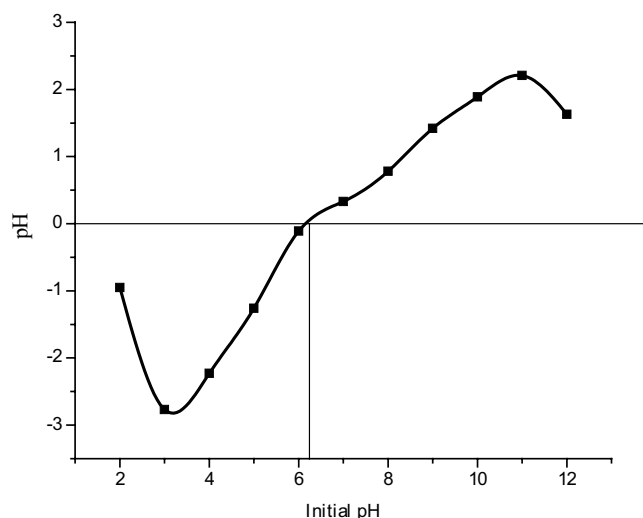
LLP adsorbent dosage on color removal is analyzed by varying the amount of adsorbent from 2–12 g L^{-1} at pH 6. From the Fig. 5, it can be seen that the decolorization efficiency of CR increases from 46.54% to 89.94%, but the equilibrium dye concentration in the solution (C_e) decreases from 133.65 to 25.15 mg L^{-1} with the increase in the adsorbent dosage from 2 to 12 g L^{-1}. This is because the increase in the adsorbent dosage results in an increase in the availability of surface area and hence an increase in the number of active sites available for the adsorption of CR dye [33]. In other words, at higher adsorbent-to-dye concentration ratios, adsorption onto the particle surface is very rapid, thus producing a lower adsorbate concentration in the solution, compared to that obtained for a lower adsorbent-to-dye concentration ratio. However, when the equilibrium adsorption capacity is expressed in mg dye adsorbed per gram of the adsorbent at equilibrium (q_e), the capacity decreases from 58.17 to 18.74 mg g^{-1} with the increase in the adsorbent dosage. This is mainly due to the split in the flux or concentration gradient between the dye concentration in the solution and that at the surface of the adsorbent. Thus, the competition for the availability of active sites for the adsorption of dye decreases with the increase in the adsorbent dosage (increase in unsaturation of adsorption binding sites in the solid surface) [29]. This phenomenon may be due to, adsorbent particle interactions, such as aggregation or overlapping of adsorption sites, resulting from high adsorbent concentration. Such aggregation would lead to a decrease in the total active surface area of the adsorbent and an increase in diffusion path length [7].

3.3.3. Effect of adsorbent particle size

The effect of particle size on adsorption of CR onto LLP adsorbent is shown in Fig. S4. The % color removal of dye is highly dependent on the adsorbent particle size. The results show that the decolorization of CR decreased
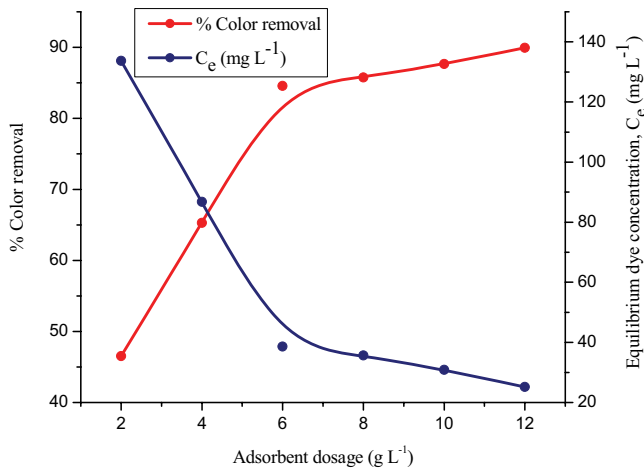
Fig. 5. Effect of LLP adsorbent dosage on CR dye adsorption. (Initial pH: 6; initial dye concentration: 250 mg L^{-1}; LLP adsorbent particle size: 93.80 μm; agitation speed: 150 rpm; temperature: 303 K; contact time: 24 h).

gradually from 89.12% to 56.44% with an increase in adsorbent particle size from 42 to 534 μm. It is observed that specific surface area is more for smaller particles. This relationship indicates that powdered adsorbent would be advantageous over granular particles. Also, the smaller particles will have a shorter diffusion path, thus allowing the dye molecule to pierce deeper into the adsorbent particle rapidly, resulting in a higher % adsorption [16].

3.3.4. Effect of agitation speed

The agitation speed in a batch adsorption process is essential to overcome the external diffusion resistance. The influence of agitation speed on decolorization efficiency was studied by varying the agitation speed from 0 to 250 rpm at 303 K. Fig. S5 shows that the color removal of CR increased from 42.38% to 86.65% with increasing agitation speed. The increase in removal efficiency may be due to enhanced turbulence attributable to the reduction in the thickness of the film surrounding the particles of LLP adsorbent, thus increasing external film diffusion and uptake of CR dye molecules [16]. This phenomenon may be explained by the increasing contact surface of the adsorbent-dye solution and favoring the transfer of dye molecules to the binding sites of the adsorbent.

3.4. Analysis of factorial experimental design and optimization of process parameters

Various groups of independent variables are used to study the mutual effect of different parameters using statistically designed experiments. The comparison of predicted response values with 31 sets of batch adsorption experimental results is reported in Table 2. The results were analysed by analysis of variance (ANOVA) and are given in Table S3. The probability level, *P*, was used to verify the significance of each of the interactions among the factors and *T*-tests were applied to evaluate the importance of the regression

Table 2
Four-factor full factorial CCD matrix for CR dye removal by LLP adsorbent

Run no.	X_1	X_2 (g L^{-1})	X_3 (μm)	X_4 (rpm)	% CR color removal	
					Experiment	Predicted
1	0	2	0	0	87.84	82.15
2	0	–2	0	0	51.12	52.02
3	1	1	1	–1	81.16	82.54
4	0	0	0	0	83.92	84.07
5	0	0	2	0	75.62	74.73
6	0	0	0	0	84.16	84.07
7	–1	1	–1	–1	83.54	85.87
8	–2	0	0	0	87.69	83.92
9	–1	–1	–1	1	78.92	80.41
10	1	1	1	1	79.82	80.55
11	0	0	0	0	84.22	84.07
12	–1	–1	1	1	68.28	69.53
13	0	0	0	–2	69.38	70.07
14	0	0	0	0	84.12	84.07
15	1	–1	1	1	67.82	68.36
16	0	0	–2	0	89.52	85.61
17	–1	1	1	–1	80.16	80.78
18	–1	1	–1	1	87.84	90.50
19	–1	1	1	1	72.59	75.46
20	1	1	–1	–1	82.54	81.86
21	1	–1	1	–1	63.22	62.50
22	1	–1	–1	–1	60.34	59.34
23	–1	–1	–1	–1	66.72	67.93
24	0	0	0	0	84.00	84.07
25	0	0	0	2	86.04	80.56
26	2	0	0	0	80.45	79.42
27	0	0	0	0	83.98	84.07
28	1	–1	–1	1	72.84	74.15
29	1	1	–1	1	85.56	89.49
30	–1	–1	1	–1	67.05	65.99
31	0	0	0	0	84.06	84.07

coefficient. Lower values of *P* (*P* < 0.05) and larger values of *T* for linear, square, and interaction effects are more significant in the chosen model at the corresponding coefficient terms. The coefficient for the linear effect of adsorbent dosage (X_2) is the first important factor (*P* = 0.000). Adsorbent particle size (X_3) and agitation speed (X_4) are the second important factor (*P* = 0.010). The coefficient for the linear effect of initial pH (X_1) of the dye solution did not signify the effect on color removal (*P* = 0.092). The coefficients of the quadratic effect of X_2 and X_4 are the first and second important factors (*P* = 0.000, *P* = 0.002) respectively. The coefficients of the quadratic effect of the variables X_1 and X_3 are not significant. The coefficients of the interaction effects of X_3X_4 and X_2X_3 are the first and second important factors (*P* = 0.010, 0.021), respectively. However, the coefficients of the other interactive effects (X_1X_2, X_1X_3, X_1X_4,

X_2X_3) among the variables did not appear to be significant. The regression model Eq. (25) for % CR dye removal is:

$$\% \text{ CR removal} = 84.0657 - 1.1233X_1 + 7.5325X_2 - 2.7217X_3 +$$
$$2.6225X_4 - 0.5989X_1^2 - 4.2464X_2^2 - 0.9739X_3^2 - 2.1889X_4^2 +$$
$$1.3138X_1X_2 + 1.2725X_1X_3 + 0.5812X_1X_4 - 0.7887X_2X_3 -$$
$$1.9650X_2X_4 - 2.2363X_3X_4 \qquad (25)$$

The suitability of the response surface model is assessed by the values of the regression coefficient (R^2), coefficient of variation, adequate precision and by the analysis of lack of fit. The regression coefficient, R^2 indicates the goodness of fit of experimental data and the predicted responses. The predicted values of % color removal match the experimental data reasonably well with R^2 of 0.9440, which indicates that 94.40% of the variations in response could be explained by this model. It also means that the model does not explain only about 5.60% of the variation. Adjusted R^2 (0.8951) is a tool to measure the goodness of fit, but it is more suitable for comparing the model with various independent variables. It corrects the R^2 value for the number of terms in the model and the sample size by using the degrees of freedom in its computations. Predicted R^2 (0.6778) can prevent overfitting the model and can be calculated from the predicted residual sum of squares (PRESS) statistics. Larger values of predicted R^2 suggest models of greater predictive ability. This may indicate that an overfitted model will not predict any new observations nearly as well as it fits the existing data. The term PRESS statistics is used to predict the responses of a new experiment and the smaller value of PRESS is more ideal [18,19]. The adequacy of the model is evaluated by the residual error which measures the difference between actual and the predicted response values. A lower value of RMSE (2.209) and AAD (1.932%) yields the best fit model equation. The repetition of central points was used to obtain the standard error of the coefficients. The ANOVA table shows the residual error, which measures the elements of variation in the response that cannot be explained by the model, and their occurrence in a normal distribution (Fig. not shown).

3.4.1. Contour and response surface plots

Contour and response surface plots are used to study the mutual interactions among the variables and to measure the maximum response level of each variable. An elliptical shaped contour plot for % color removal of CR as shown in Figs. 6a–d. The coordinates of the central point in each of these contour plots indicate the optimal value of the respective constituents. Fig. 6a shows that the contour plot of % color removal from the aqueous solution as a function of initial pH and LLP adsorbent dosage. The % color removal occurs when the adsorbent dosage ranges between 5 and 9.5 g L⁻¹, initial pH in the range of 5.6–6.4, and the effect is insignificant. Fig. 6b shows that the maximum predicted response occurs when the LLP adsorbent particle size ranges between 42 and 55 μm and the agitation speed ranges from 176 to 220 rpm. Fig. 6c shows that the maximum predicted yield occurs when the initial pH of the dye solution ranges between 5.6 and 5.65, and the LLP adsorbent particle size

in the range of 42–48.5 μm. Fig. 6d shows that the maximum predicted % color removal occurs when the agitation speed ranges between 89 and 220 rpm and the LLP adsorbent dosage ranges from 5 to 10 g L⁻¹, and the effect is not very significant. A similar observation has been reported elsewhere [19]. The three-dimensional response surface plot was used to understand the main and interaction effects among the variables and to determine the optimum response level of each variable. Response surface plots are developed as a function of two factors while maintaining all other factors at fixed levels. The optimum conditions of the relative variables will resemble with the coordinates of the central point in the upmost level in each of these figures [20]. The response surface curves for % color removal of CR as shown in Figs. 7a–d. Fig. 7a shows the surface plot of the response variable as a function of initial pH and LLP adsorbent dosage. It clearly shows that the decolorization efficiency increased with a decrease in the pH and with an increase in adsorbent dosage. The value of pH in the range of 5.6–6.4 does not have a significant effect, while an adsorbent dosage ranging between 2 and 10 g L⁻¹ has a significant effect on the decolorization of CR. Fig. 7b shows that with a decrease in the adsorbent particle size and increase in agitation speed, the % color removal improves. The response surface plot of agitation speed in the range of 176–220 rpm does not have a significant effect, while an adsorbent particle size ranging between 42 and 146 μm has a significant effect on the maximum % adsorption of the CR dye. Fig. 7c exhibits that the % color removal of CR increased with a decrease in initial pH of the dye solution and adsorbent particle size. The response surface plot of adsorbent particle size ranging between 42 and 146 μm vs. the initial pH in the range of 5.6–6.4 shows a significant effect on color removal. Similarly, Fig. 7d shows that with an increase in the adsorbent dosage and agitation speed, the decolorization efficiency improves. The response surface plot of agitation speed in the range of 80–220 rpm vs. the adsorbent dosage in the ranges between 2 and 10 g L⁻¹ shows a significant effect on color removal of CR from aqueous solution. The optimal response values found from these plots are closely related to the values obtained from the experiment and regression model equation.

3.4.2. Process model validation

Three solutions with different values of ideal initial conditions are used to predict the optimum conditions for CR dye decolorization by LLP adsorbent which is shown in Table 3. Various experiments were performed under fixed conditions and the results were compared to the predicted responses. The maximum color removal efficiency (89.52%) was obtained in experiment number 3. The optimal values of the process independent variables for maximal response are given in Table 4. The comparison between experimental and predicted responses shows a good relationship between them, and it suggests that the empirical model resulting from the design could as well be used for describing the relation between process factors and the response in CR dye decolorization. The optimization studies clearly reveal that RSM is a good method to predict the ideal conditions for maximum decolorization efficiency.
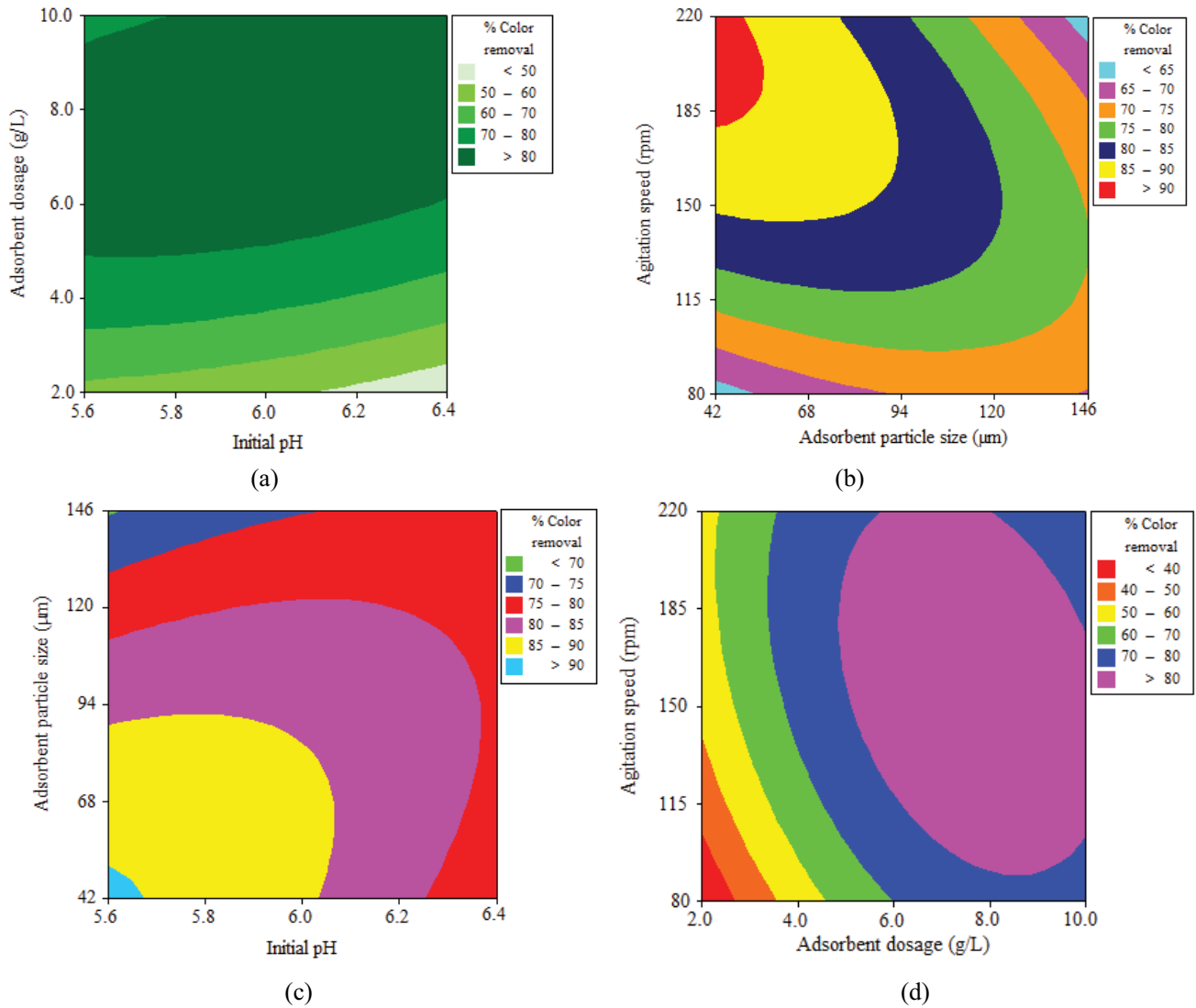
Fig. 6. Contour plots for the interactive effect of (a) adsorbent dosage and initial pH, (b) agitation speed and adsorbent particle size, (c) adsorbent particle size and initial pH, and (d) agitation speed and adsorbent dosage on color removal of CR dye.

Table 3
Validation of process model for % color removal of CR

Expt.	Process parameters with operating conditions				CR color removal (%)	
	X_1	X_2 (g L^{-1})	X_3 (µm)	X_4 (rpm)	Actual value	Predicted value
1	6.0	6.0	42	150	89.52	87.34
2	6.2	8.0	68	115	82.54	80.67
3	5.8	8.0	120	185	72.59	73.84

3.5. Inference from adsorption isotherm models

The linearized Langmuir, Freundlich, and Temkin isotherms plots for the adsorption of CR dye by the LLP adsorbent at 303 K are shown in Figs. 8, S6 and S7, respectively. The results of model parameters obtained from the regressive analysis of these plots are reported in Table 5.

The best-fitted isotherm models are chosen in the order of prediction precision: Langmuir > Temkin > Freundlich isotherms. From Table 5, a higher value of the regression coefficient ($R^2 = 0.9999$) and lower value of chi-square ($\chi^2 = 0.04444$) were found for the Langmuir model, compared to the Temkin isotherm ($R^2 = 0.9858$, $\chi^2 = 1.0633$) and Freundlich ($R^2 = 0.9765$, $\chi^2 = 6.3418$) models. This tells us
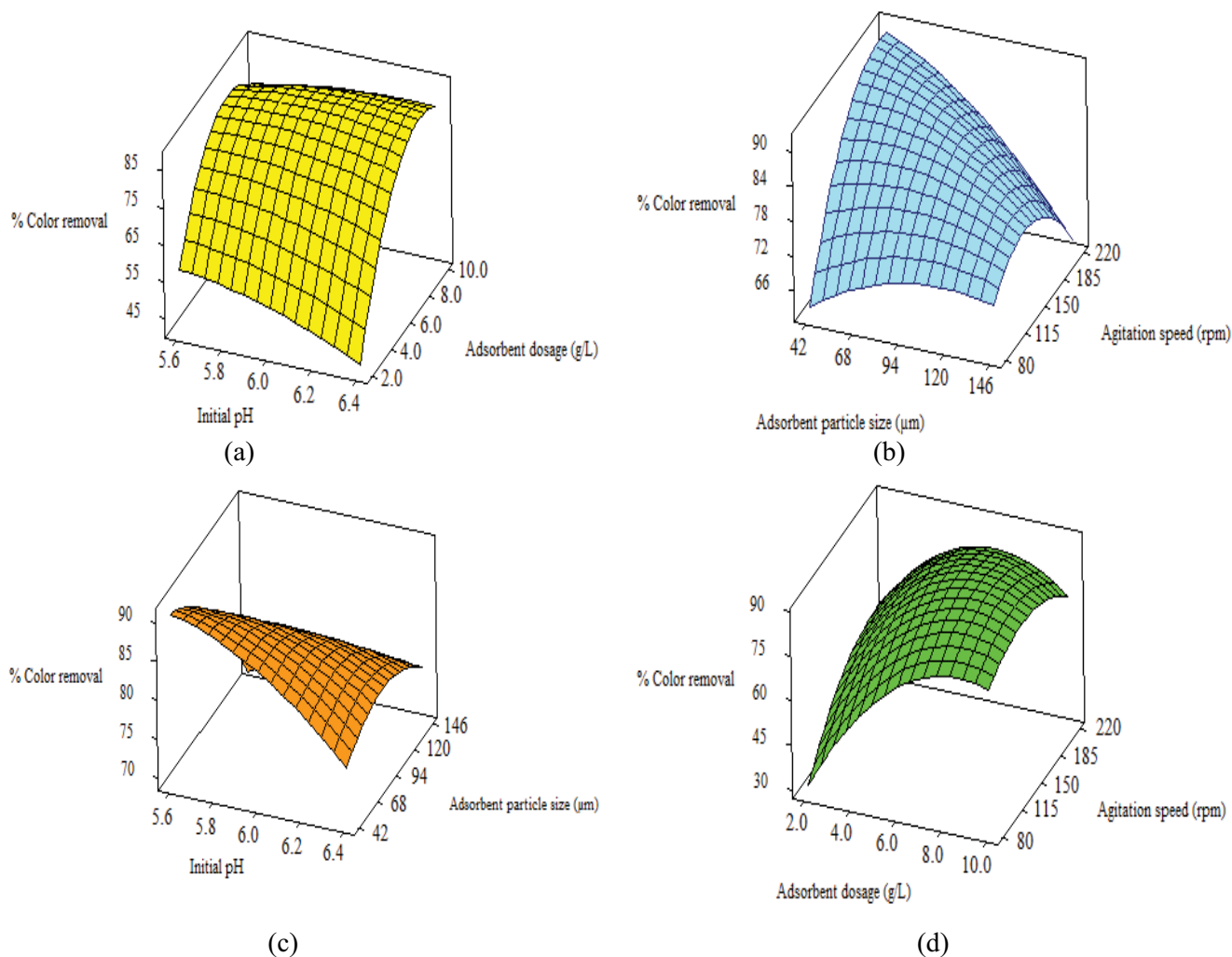
Fig. 7. Response surface plots for the interactive effect of (a) adsorbent dosage and initial pH, (b) agitation speed and adsorbent particle size, (c) adsorbent particle size and initial pH, and (d) agitation speed and adsorbent dosage on color removal of CR dye.

Table 4
Optimal values of the process independent variables for maximum % color removal of CR dye

Process parameters	Optimum value	CR color removal (%)
Initial pH (X_1)	6.0	
LLP adsorbent dosage, g L^{-1} (X_2)	6.0	
LLP adsorbent particle size, μm (X_3)	42	89.52
Agitation speed, rpm (X_4)	150	

that the equilibrium dye uptake (q_e) data fits very well with the Langmuir isotherm model. According to the assumptions of the Langmuir isotherm, the adsorption is homogeneous in nature with the formation of unimolecular layer at binding sites [2]. The maximum monolayer capacity (q_{max}) and Langmuir isotherm parameter (K_L) of the LLP adsorbent (q_{max}) are estimated to be 45.89 mg g^{-1} and 0.135 L mg^{-1}, respectively at 303 K. Whereas the value of q_{max} and K_L of commercial activated carbon for the removal of CR are reported to be 300 mg g^{-1} and 6.49 × 10^{-3} L mg^{-1},

respectively at 303 K [36]. The calculated R_L values obtained using LLP adsorbent at various initial adsorbate concentrations are shown in Fig. S8. It shows that the adsorption is more favorable at higher concentrations. Also, the value of the separation factor, R_L fell in the range of 0–1 at all initial adsorbate concentration (50–300 mg L^{-1}) and this confirms the favorable uptake of the adsorption process. At higher concentration, the adsorption process was found to be more favorable. The value of Freundlich constant, n (2.148) is between 1 and 10 which again proved that the
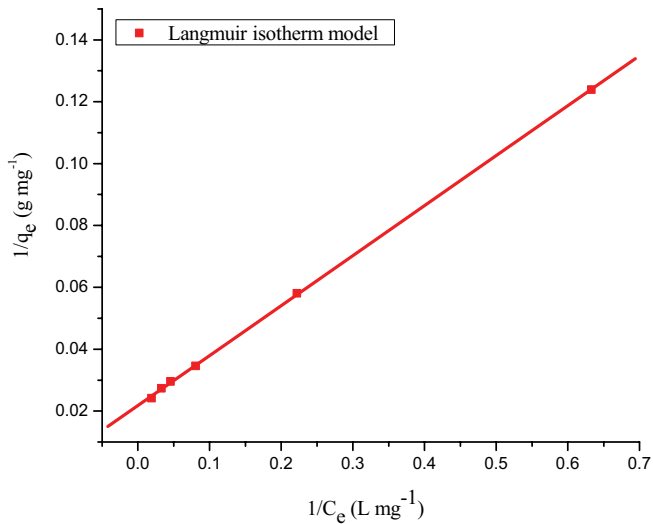
Fig. 8. Langmuir isotherm plot for adsorption of CR dye onto LLP adsorbent. (Initial pH: 6; initial dye concentration: 50–300 mg L^{-1}; LLP adsorbent dosage: 6 g L^{-1}; LLP adsorbent particle size: 93.80 μm; agitation speed: 150 rpm; temperature: 303 K; contact time: 24 h).

Table 5
Adsorption isotherm model parameters for CR dye adsorption onto LLP adsorbent

Isotherm	Model parameters	Values	Model equation
Freundlich	n	2.149	
	K_F (L g^{-1})	2.416	$q_e = 2.416 C_e^{0.4653}$
	R^2	0.9765	
	χ^2	6.3418	
Langmuir	q_{max} (mg g^{-1})	45.892	
	K_L (L mg^{-1})	0.1348	$q_e = \dfrac{6.19\,C_e}{1+0.1348\,C_e}$
	R^2	0.9999	
	χ^2	0.0444	
Temkin	K_T (L g–1)	1.2328	
	b_T (kJ mol^{-1})	0.2640	$q_e = 9.539 \ln\left(1.2328\,C_e\right)$
	R^2	0.9858	
	χ^2	1.0633	

Table 6
Comparison of maximum monolayer adsorption capacity of CR dye onto various adsorbents

Adsorbent	Maximum adsorption capacity q_{max} (mg g^{-1})	References
Zeolite	3.77	[37]
Waste red mud	4.05	[38]
Kaolin	5.44	[37]
Activated carbon from coir pith	6.70	[39]
Acid activated red mud	7.08	[40]
Rubber seeds	9.82	[41]
Bagasse fly ash	11.88	[42]
Pineapple plant stem	11.97	[43]
Montmorillonite	12.70	[44]
Orange peel	14.00	[45]
Rice bran	14.63	[46]
Aspergillus niger	14.72	[47]
Luffa cylindrica cellulosic fiber	17.39	[48]
Banana peel	18.20	[45]
Acid activated bentonite	20.70	[49]
Orange peel	22.44	[50]
Anilinepropylsilica xerogel	22.62	[51]
Wheat bran	22.73	[46]
Natural pumice	27.32	[52]
Fe–Zn bimetallic nanoparticles	28.56	[53]
Eucalyptus wood sawdust	31.25	[54]
Chitosan/TiO$_2$ nanocomposite	32.00	[55]
Apricot stone activated carbon	32.85	[56]
NaOH treated jute fibre	33.69	[11]
Jute stick powder	35.70	[57]
Sodium bentonite	35.84	[37]
Sugarcane bagasse	38.20	[58]
Cattail root	38.79	[59]
Neem leaf powder	41.24	[60]
Cross-linked cellulose dialdehyde	42.03	[61]
Chrysanthemum indicum flower	43.47	[62]
Lotus leaf powder	45.89	Present study

adsorption is favorable. The q_{max} of the LLP adsorbent for the removal of CR was compared with those of other adsorbents reported in the literature and the values are shown in Table 6. It can be inferred from the table that the prepared LLP adsorbent has superior adsorption capacity for the decolorization of CR from aqueous solutions in comparison with the reported adsorbents. The intensity of the peaks of the synthetic CR dye effluent was measured before and after adsorption. The intensity of the peaks declined after treatment which indicates that CR dye molecules were adsorbed on the LLP adsorbent surface in 24 h (Fig. S9). After treatment, the peak wavelength (λ_{max}) of treated synthetic CR dye effluent was similar to the original untreated CR dye wavelength of concentration 100 mg L^{-1}.

3.6. Inference from thermodynamic analysis for the adsorption of CR

The results for the amount of dye adsorbed onto LLP adsorbent at equilibrium (q_e) with equilibrium adsorbate concentrations (C_e) and various temperatures are shown in Fig. S10. It shows that the equilibrium adsorption capacity increases with the increase in temperature. The q_{max} of CR dye increased from 45.89 mg g^{-1} at 303 K to 62.54 mg g^{-1} at 323 K. This is because of the pore volume of the LLP adsorbent particles increases at higher temperatures [26]. The pore volume increased from 7.1 mm^3 g^{-1} at room temperature (303 K) to 12.1 mm^3 g^{-1} at 323 K. The increase in decolorization efficiency, and equilibrium dye uptake onto

the particle surface at higher temperature suggests that the adsorption process is rapid and endothermic in nature. This phenomenon may be due to an increase in the diffusion of dye molecules across the boundary layer and in the internal pores of the solid adsorbent particle leading to a reduction in the swelling of the adsorbate molecules with increasing temperatures [7]. An increasing number of dye molecules may also gain adequate energy to interact with binding sites at the solid particle surface. The enhancement in the adsorption capacity at higher temperatures might be due to the chemical interaction between dye molecules and adsorbent or generation of some new adsorption binding sites on the particle surface. In addition, the increasing temperature may produce a swelling effect within the inner structure of the adsorbent thus allowing more adsorbate molecules to diffuse additionally [8]. The thermodynamic parameters are calculated from the Van't Hoff plot (Fig. 9), and the values are reported in Table 7. It shows that the values of ΔG decreased with the increase in temperature, suggesting that the adsorption was a spontaneous process. The values of ΔG becomes more negative with increasing temperature, suggesting that higher temperatures promote the adsorption of dye molecules. A positive value of ΔH again proves that the adsorption of CR onto the LLP adsorbent was an endothermic process. The positive value of ΔS suggests increased
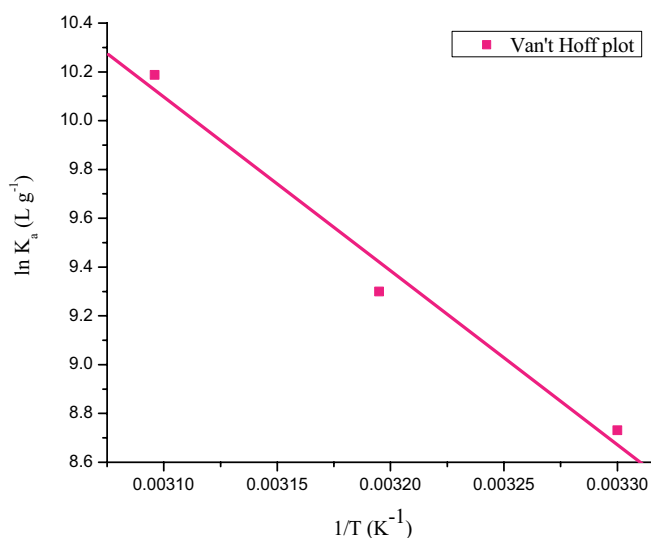
randomness of dye molecules on the adsorbent particle surface than in the dye solution. The activation energy (E_a) of adsorption was determined from the Arrhenius plot (Fig. S11) and found to be 44.14 kJ mol^{-1} with an adsorbate concentration of 200 mg L^{-1}. The E_a values are found in the ranges between 42.18–53.36 kJ mol^{-1} at various adsorbate concentrations and it is given in Table S4. The value of ΔH (59.225 kJ mol^{-1}) and activation energy (46.487 kJ mol^{-1}) indicates that dye adsorption onto the LLP adsorbent is a chemisorptive process [63]. It may confirm that the bonding energy between adsorbate molecules and active sites on the adsorbent is stronger at higher temperatures [53].

3.7. Inference from adsorption kinetic models

The adsorption kinetics for the removal of CR onto the LLP adsorbent was rapid in the initial stages of the process. However, the dye uptake rate later decreased progressively with time. The active sites saturated at approximately 4 h for 50 mg L^{-1}, 5 h for 100 mg L^{-1}, 6 h for 150 mg L^{-1}, 7 h for 200 mg L^{-1}, 8 h for 250 mg L^{-1} and 9 h for 300 mg L^{-1}. Fig. S12 shows that the % color removal of CR gradually decreased from 96.84% to 82.36%, but the value of q_e increased from 8.07 to 41.34 mg g^{-1} with the increase in adsorbate concentration from 50 to 300 mg L^{-1}. The decrease in decolorization efficiency with an increase in dye concentration is due to the accumulation of adsorbate in the vacant sites of the adsorbent (available binding sites on the adsorbent surface were saturated) and increased competition between the more adsorbate molecules at the fixed active sites of the adsorbent. Hence, the lack of available active sites in the adsorbent surface leads to a decrease in the % color removal [31]. The value of the initial adsorption rate (h) increased from 1.528 to 11.484 mg g^{-1} min^{-1} with an increase in initial dye concentration. The increase in the value of q_e and h is because of an increase in concentration difference among the adsorbate concentration in the solution and the surface of the solid particle. This concentration gradient acts as a driving force for the diffusion of dye molecules from the bulk solution to the particle surface [10]. The linearized form of the pseudo-first-order and pseudo-second-order kinetic plots are shown in Figs. S13 and 10, respectively and the results obtained from these plots are shown in Table 8. It was observed that a lower value of SD (0.089%–0.486%) and higher value of R^2 (0.9998) exists in the concentration ranging between 50–300 mg L^{-1}, indicating that the experimental data for adsorption of CR onto LLP adsorbent appropriately fits the pseudo-second-order model. In addition, the predicted q_e values from the pseudo-second-order model are closer to the experimental values at various adsorbate

Fig. 9. Van't Hoff plot for adsorption of CR dye onto LLP adsorbent. (Initial pH: 6; initial dye concentration: 50–300 mg L^{-1}; LLP adsorbent dosage: 6 g L^{-1}; LLP adsorbent particle size: 93.80 μm; agitation speed: 150 rpm; contact time: 24 h).

Table 7
Thermodynamic parameters for the adsorption of CR dye onto LLP adsorbent

Temperature (K)	Maximum adsorption capacity q_{max} (mg g^{-1})	Thermodynamic parameters		
		ΔG (kJ mol^{-1})	ΔH (kJ mol^{-1})	ΔS (kJ mol^{-1} K^{-1})
303	45.892	−21.994		
313	51.813	−23.448	59.225	0.2675
323	62.539	−27.358		

Table 8
Kinetic parameters for the adsorption of CR dye onto LLP adsorbent

Initial dye concentration (mg L^{-1})	$q_{e,\text{expt.}}$ (mg g^{-1})	Pseudo-first-order kinetic model				Pseudo-second-order kinetic model				
		$q_{e,\text{cal.}}$ (mg g^{-1})	K_1 (min^{-1})	SD (%)	R^2	$q_{e,\text{cal.}}$ (mg g^{-1})	h (mg g^{-1} min^{-1})	K_2 (g mg^{-1} min^{-1})	SD (%)	R^2
50	8.069	2.384	0.0178	18.830	0.9866	8.187	1.528	0.0235	0.389	0.9997
100	17.238	4.273	0.0156	19.552	0.9862	16.129	4.025	0.0135	1.720	0.9996
150	28.910	4.234	0.0121	21.791	0.9449	26.020	10.066	0.0120	2.672	0.9999
200	33.807	4.325	0.0082	22.832	0.9395	30.700	10.758	0.0093	2.456	0.9999
250	36.576	5.433	0.0069	22.755	0.9406	36.536	10.996	0.0082	0.029	0.9998
300	41.339	6.693	0.0045	22.398	0.9475	41.477	11.240	0.0067	0.089	0.9999

concentrations than those from the pseudo-first-order model. The q_e values evaluated from the pseudo-first-order kinetic model largely deviated from the experimental values, a higher value of SD and lower value of R^2 suggests that this model is not valid for adsorption of CR. The above results suggest that the adsorption kinetics of CR onto LLP adsorbent can be best described by the pseudo-second-order rate equation and can be considered to be endothermic chemisorption. The adsorption experiments were performed at pH 6 and the zero-potential charge of the adsorbent has been found to occur at pH 6.2. Hence at pH 6.2, the active sites in the adsorbent are positively charged which promotes the electrostatic attraction of negatively charged anionic dye molecules. The adsorption process is chemisorption, involving strong binding forces via the sharing of electrons among the adsorbent and adsorbate molecules as covalent forces [58]. The calculated value of E_a and ΔH in the studied adsorption process again confirms the involvement of the chemisorption mechanism and it is given in the above section 3.6. The rate constant, K_2, decreased from 0.0234

to 6.572×10^{-3} g mg^{-1} min^{-1} with an increase in adsorbate concentration from 50 to 300 mg L^{-1}. This may be due to decreased competition at the active sites on the adsorbent surface at lower concentrations and increased competition for the binding sites at higher concentrations [55].

3.8. Inference from adsorption rate mechanism

The pore diffusion plot for the adsorption of CR onto the LLP adsorbent is shown in Fig. 11 and the model parameters are reported in Table S5. From Fig. 11, the first region follows the external boundary layer diffusion of the adsorbate and the process is rapid. Nearly, 65%–70% of CR was taken up by LLP adsorbent within a $t^{1/2}$ value of 10 min, indicating a strong electrostatic interaction between adsorbate molecules and the external surface of the adsorbent. Second, region is attributed to the progressive adsorption stage, where pore diffusion is rate controlling. It indicates the diffusion of the adsorbate molecules through the pores
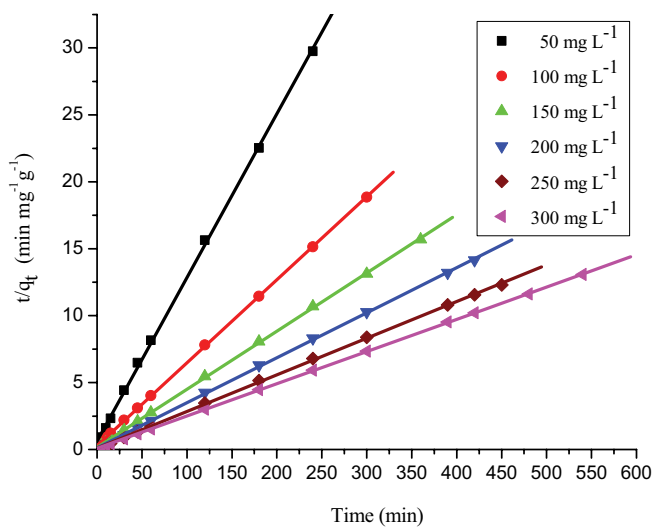

Fig. 10. Ho's pseudo-second-order kinetic plot for adsorption of CR dye onto LLP adsorbent. (Initial pH: 6; initial dye concentration: 50–300 mg L^{-1}; LLP adsorbent dosage: 6 g L^{-1}; LLP adsorbent particle size: 93.80 μm; agitation speed: 150 rpm; temperature: 303 K; contact time: 24 h).
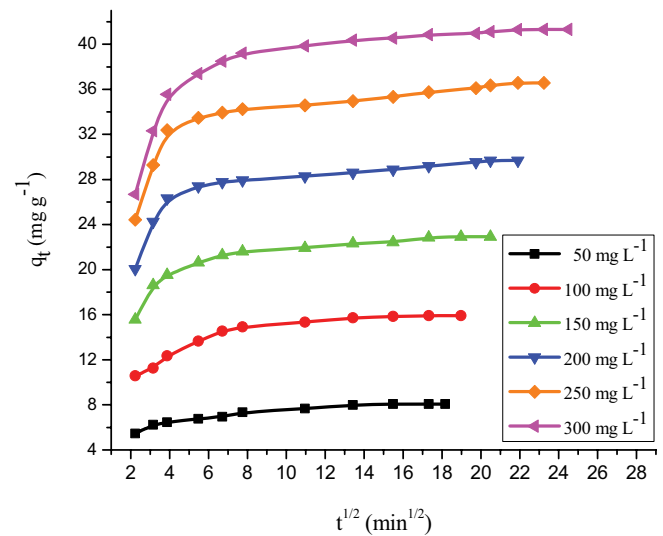

Fig. 11. Intraparticle diffusion plot for adsorption of CR dye onto LLP adsorbent. (Initial pH: 6; initial dye concentration: 50–300 mg L^{-1}; LLP adsorbent particle size: 93.80 μm; agitation speed: 150 rpm; temperature: 303 K; contact time: 24 h).

of the adsorbent. The third region refers to the final saturation stage and the pore diffusion starts to slow down due to the low adsorbate concentration in the aqueous solution [64]. Extrapolation of the second section back to the *y*-axis yields the value of *C*. A larger boundary layer diffusion effect is indicated by a large intercept value. The decrease in intercept value denotes that the process is mainly controlled by pore diffusion, with a slight effect of external film diffusion. Also, the plots at each concentration did not pass through the origin, indicating that the pore diffusion was not only the rate-limiting step [65]. The value of K_i obtained from these plots increased with an increase in initial adsorbate concentration. From Table S4, the value of R^2 of the intraparticle diffusion model for various adsorbate concentrations is lower than the pseudo-second-order kinetic model. This again proves that the experimental data fit well with the pseudo-second-order kinetic model. Therefore, the overall rate of the adsorption is mostly controlled by external film diffusion, followed by a small effect of pore diffusion of CR dye anions to the particle's interior surface. It was found that the adsorption process may be controlled due to external film diffusion at initial phases and as the solid particles are loaded with adsorbate molecules, it may be controlled due to pore diffusion at later phases. In addition, the experimental data were analyzed using Bangham and Boyd kinetic expressions. The Boyd plot (Fig. 12) and Bangham plot (Fig. S14) are found to be a straight line that does not pass through the origin suggesting that the external film diffusion mostly governs the overall rate of the reaction.

3.9. Inference from desorption studies and reusability of LLP adsorbent

Desorption experiments are performed for the removal of CR from LLP adsorbent loaded with dye molecules and results are shown in Fig. S15 and Table S6. It shows that the % of CR dye desorbed reduced with an increasing number of runs. The % desorption in all the runs was determined to be in the order of methanol > ethanol > 1 M NaOH > acetone > butanol with various desorbing reagents in separate batches. It was found that up to a maximum of 56.852% of the dye could be desorbed using the solvent methanol in the third run, compared with other desorbing reagents. This may be due to the low volume of the desorbing reagent used or lack of agitation speed, which may prevent further release of bound dye anions to the desorbing reagent [7].

The regenerated LLP adsorbent was added to the dye solution of concentration 200 mg L⁻¹. The regenerated adsorbent was tested in the second and third runs. The results obtained from reusability studies for the adsorption of CR in various runs are shown in Fig. S16 and Table S7. It shows that, in comparison to the first run, 73.485% adsorption was maintained after 24 h in the second run and 65.364% in the third run (using the solvent methanol in the desorption process). This may be because of the incomplete desorption of the bound adsorbate molecules from the solid particle surface (adsorbent active sites are almost blocked with CR dye molecules) and lack of binding sites on the adsorbent [12]. Therefore, the dye adsorption % progressively decreased with an increase in the number of runs.
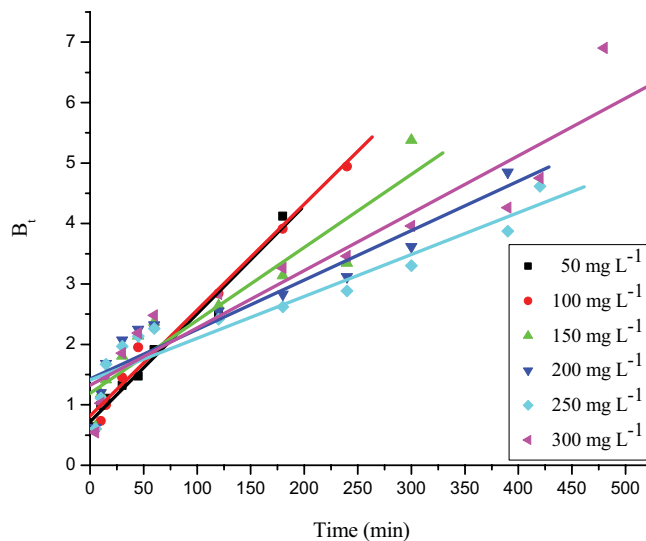

Fig. 12. Boyd plot for adsorption of CR dye onto LLP adsorbent. (Initial pH: 6; initial dye concentration: 50–300 mg L⁻¹; LLP adsorbent dosage: 6 g L⁻¹; adsorbent particle size: 93.80 μm; agitation speed: 150 rpm; temperature: 303 K; contact time: 24 h).
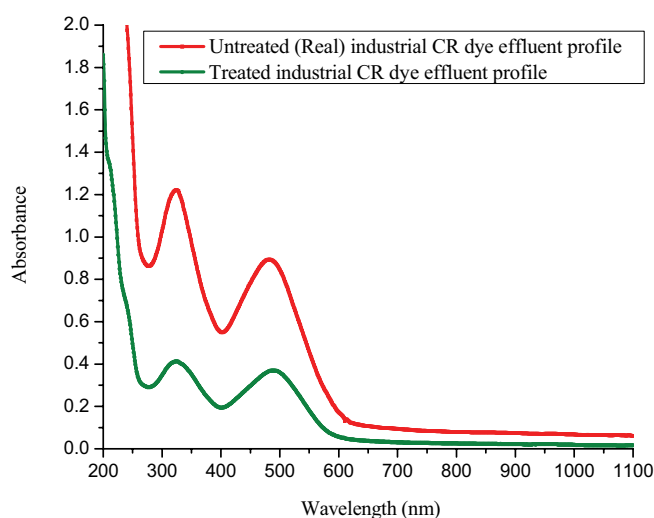

Fig. 13. Industrial CR dye effluent adsorption profile obtained in batch studies using LLP adsorbent with the untreated effluent profile. (Initial pH: 8.65; initial COD: 1845 mg L⁻¹; initial adsorbate concentration: 215 mg L⁻¹; LLP adsorbent dosage: 6 g L⁻¹; LLP adsorbent particle size: 93.80 μm; agitation speed: 150 rpm; temperature: 303 K; contact time: 24 h).

3.10. Analysis of industrial CR dye effluent using LLP adsorbent

The real textile CR dye effluent was collected from Bright Traders, Erode District, Tamilnadu State, India. The industrial raw effluent was centrifuged to separate the salt content, and dispersed solids, due to the high COD value of the effluent (1,845 mg L⁻¹). The pH of the raw effluent was 8.65. The optimized value of various process parameters that are obtained from CCD was used to remove COD from industrial CR dye effluents. The initial adsorbate concentration was measured and it was found to be 215 mg L⁻¹ and

the COD removal efficiency of industrial dye effluent was 67.35%. The intensity of the peaks of industrial dye effluent was measured before and after adsorption. The intensity of peaks declined considerably after treatment using LLP adsorbent (Fig. 13). The above results showed that the lotus leaf fine powder was a useful adsorbent for effective adsorption of CR from industrial effluents. Therefore, the present research work is important for adsorption studies and contributes to the pollution treatment application.

4. Conclusion

The removal of CR from an aqueous solution using lotus leaf powder adsorbent has been studied in batch mode. The prepared adsorbent was characterized using particle size, ATR, FESEM/EDS, BET, TGA and proximate analysis. The peaks in ATR studies revealed that the surface of the adsorbent contains abundant hydroxyl, methyl, alkyne, and carbonyl groups. The % color removal of CR was found to decrease with an increase in initial pH, adsorbate concentration and particle size. It increased with an increase in adsorbent dosage and agitation speed. The equilibrium adsorption capacity increased with the increase in initial adsorbate concentration and temperature but decreased with an increase in the mass of adsorbent. The Langmuir isotherm model and the pseudo-second-order kinetic model fitted very well to the adsorption equilibrium and kinetic data, respectively. The equilibrium data confirming the monolayer adsorption of CR onto adsorbent with a maximum monolayer adsorption capacity (q_{max}) of 45.89 mg g^{-1} at 303 K. The value of Freundlich constant and dimensionless separation factor showed that the process was favorable. Thermodynamic parameters revealed that the process is endothermic and spontaneous in nature and, thus, the adsorption is favorable at higher temperatures. The value of E_a and ΔH suggests that the adsorption can be characterized as a chemisorption process. The adsorption mechanism implies that the external film diffusion controlled the dye uptake in the earlier stages, followed by pore diffusion, which controlled the rate at later stages. The Boyd and Bangham plots confirmed that the process is controlled by external film diffusion, which is the slowest step that mainly governs the rate of the reaction. Desorption studies on loaded adsorbent showed that the maximum % of CR dye could be desorbed using the solvent methanol. It shows that the % desorption decreased with the increase in the number of runs for all various desorbing reagents. The regenerated adsorbent can be used effectively up to three cycles to adsorb CR dye in aqueous solutions with a considerable reduction in adsorption efficiency. The experimental results concluded that LLP is an effective adsorbent for the removal of color from synthetic and industrial CR dye from wastewater. The higher adsorption efficiency of industrial CR dye effluent suggests that the lotus leaf fine powder may be used effectively to decolorize other anionic dyes from industrial effluents.

Symbols and abbreviations

A	—	Arrhenius frequency factor
AAD	—	Absolute average deviation
Adj. MS	—	Adjusted mean squares
Adj. SS	—	Adjusted sum of squares
ANOVA	—	Analysis of variance
ATR	—	Attenuated transmission reflector
BET	—	Brunauer–Emmett–Teller
B_t	—	Mathematical function of F
b_T	—	Adsorption energy, kJ mol^{-1}
C	—	Constant (intercept value in intraparticle diffusion model), mg g^{-1}
CCD	—	Central composite design
COD	—	Chemical oxygen demand, mg L^{-1}
CR	—	Congo red dye
C_0	—	Initial dye concentration in solution, mg L^{-1}
C_e	—	Equilibrium dye concentration in solution, mg L^{-1}
C_t	—	Dye concentration in solution at any time t, mg L^{-1}
DF	—	Degree of freedom
E_a	—	Activation energy of adsorption, kJ mol^{-1}
EDS	—	Energy-dispersive X-ray spectroscopy
F	—	Ratio of the amount of dye adsorbed at any time t to equilibrium
$F_{statistics}$	—	Fisher's 'F'-test
f	—	Number of variables
FESEM	—	Field-emission scanning electron microscopy
h	—	Initial rate of adsorption, mg g^{-1} min^{-1}
K_a	—	Adsorption equilibrium constant, L g^{-1}
K_F	—	Freundlich isotherm constant, L g^{-1}
K_i	—	Intraparticle diffusion rate constant, mg g^{-1} min$^{-1/2}$
K_L	—	Langmuir isotherm constant, L mg^{-1}
K_T	—	Temkin isotherm constant, L g^{-1}
K_1	—	Pseudo-first-order rate constant, min^{-1}
K_2	—	Pseudo-second-order rate constant, g mg^{-1} min^{-1}
k_0	—	Bangham model constant, L^2 g^{-1}
LLP	—	Lotus leaf fine powder
m	—	Mass of adsorbent per volume of solution, g L^{-1}
N	—	Numbers of experimental runs
N_P	—	Number of data points
N_0	—	Number of center points
n	—	Heterogeneity factor
P	—	Probability value
PRESS	—	Predicted residual sum of squares
q_e	—	Amount of dye adsorbed at equilibrium, mg g^{-1}
$q_{e,expt.}$	—	Experimental adsorption capacity, mg g^{-1}
$q_{e,cal.}$	—	Calculated adsorption capacity, mg g^{-1}
q_{max}	—	Theoretical monolayer maximum saturation capacity, mg g^{-1}
q_t	—	Amount of dye adsorbed on the adsorbent surface at any time t, min
R	—	Universal gas constant, 8.314 J mol^{-1} K^{-1}
R^2	—	Linear regression correlation coefficient
R_L	—	Langmuir isotherm separation factor
RMSE	—	Root mean square error
RSM	—	Response surface methodology
S	—	Value of S-chart
SD	—	Standard deviation
SE	—	Standard error of coefficient

SEM — Scanning electron microscopy
Seq. SS — Sequential sum of squares
TGA — Thermogravimetric analysis
$T_{statistics}$ — Student 'T'-test
t — Adsorption time, min
T — Temperature, K
V — Volume of dye solution, mL
W — Mass of lotus leaf fine powder adsorbent, g.
x_i — Dimensionless value of a process variable X_i
X_i — Real value of an independent variable
X_0 — Value of X_i at the center point
X_1 — Initial pH
X_2 — LLP adsorbent dosage, g L^{-1}
X_3 — LLP adsorbent particle size, μm
X_4 — Agitation speed, rpm
Y_p — Predicted response variable (% color removal)
Y_a — Actual response variable (% color removal)
ΔG — Changes in Gibbs free energy, kJ mol^{-1}
ΔH — Changes in enthalpy, kJ mol^{-1}
ΔS — Changes in entropy, kJ mol^{-1} K^{-1}
2^f — Number of factorial points
$2f$ — Axial points

Greek letters

α — Bangham model constant
β_0 — Offset term
β_i — Regression coefficients for a linear effect
β_{ii} — Regression coefficients for the quadratic effect
β_{ij} — Regression coefficients for the interaction effect
δX — Step change
χ^2 — Chi-square test value

References

[1] W.C. Wanyonyi, J.M. Onyari, P.M. Shiundu, Adsorption of Congo red dye from aqueous solutions using roots of *Eichhornia crassipes*: kinetic and equilibrium studies, Energy Procedia, 50 (2014) 862–869.

[2] A. Sharma, Z.M. Siddiqui, S. Dhar, P. Mehta, D. Pathania, Adsorptive removal of Congo red dye (CR) from aqueous solution by *Cornulaca monacantha* stem and biomass-based activated carbon: isotherm, kinetics and thermodynamics, Sep. Sci. Technol., 54 (2019) 916–929.

[3] J.M. Divya, K. Palak, P. Vairavel, Optimization, kinetics, equilibrium isotherms, and thermodynamics studies of Coomassie violet dye adsorption using *Azadirachta indica* (neem) leaf adsorbent, Desal. Water Treat., 190 (2020) 353–382.

[4] V.S. Munagapati, D.-S. Kim, Equilibrium isotherms, kinetics, and thermodynamics studies for Congo red adsorption using calcium alginate beads impregnated with nano-goethite, Ecotoxicol. Environ. Saf., 141 (2017) 226–234.

[5] K. Saeed, M. Ishaq, S. Sultan, I. Ahmad, Removal of methyl violet 2-B from aqueous solutions using untreated and magnetite-impregnated almond shell as adsorbents, Desal. Water Treat., 57 (2016) 13484–13493.

[6] Z.A. Medvedev, H.M. Crowne, M.N. Medvedeva, Age related variations of hepatocarcinogenic effect of azo dye (3'-MDAB) as linked to the level of hepatocyte polyploidization, Mech. Ageing Dev., 46 (1988) 159–174.

[7] P. Vairavel, V.R. Murty, Optimization, kinetics, equilibrium isotherms, and thermodynamics studies for Congo red dye adsorption using calcium alginate beads immobilized with dual adsorbent (*Neurospora crassa* dead fungal biomass and wheat bran), Desal. Water Treat., 97 (2017) 338–362.

[8] A. Zúñiga-Zamoraa, J.G. Mena, E. Cervantes-Gonzáleza, Removal of Congo red from the aqueous phase by chitin and chitosan from waste shrimp, Desal. Water Treat., 57 (2015) 1–12.

[9] C. Debamita, N. Rampal, J.P. Gautham, P. Vairavel, Process optimization, isotherm, kinetics, and thermodynamic studies for removal of Remazol Brilliant Blue-R dye from contaminated water using adsorption on guava leaf powder, Desal. Water Treat., 185 (2020) 318–343.

[10] A. Azari, R. Rezaei, H. Sanaeepur, Synthesis and characterization of TiO$_2$ nanoparticles loaded activated carbon for Congo red removal from wastewater: kinetic and equilibrium studies, Desal. Water Treat., 124 (2018) 308–318.

[11] A.K. Dey, U. Kumar, A. Dey, Use of response surface methodology for the optimization of process parameters for the removal of Congo red by NaOH treated jute fibre, Desal. Water Treat., 124 (2018) 308–318.

[12] P. Vairavel, V.R. Murty, Continuous fixed-bed adsorption of Congo red dye by dual adsorbent (*Neurospora crassa* dead fungal biomass and wheat bran): experimental and theoretical breakthrough curves, immobilization and reusability studies, Desal. Water Treat., 98 (2017) 276–293.

[13] M.T. Yagub, T.K. Sen, S. Afroze, H.M. Ang, Dye and its removal from aqueous solution by adsorption: a review, Adv. Colloid Interface Sci., 209 (2014) 172–184.

[14] X.L. Han, J.Y. Yuan, X.J. Ma, Adsorption of Malachite green from aqueous solutions onto lotus leaf: equilibrium, kinetic, and thermodynamic studies, Desal. Water Treat., 52 (2014) 5563–5574.

[15] K.R. Paudel, N. Panth, Phytochemical profile and biological activity of *Nelumbo nucifera*, Evidence-Based Complementary Altern. Med., 2015 (2015) 1–17, https://doi.org/10.1155/2015/789124.

[16] P. Vairavel, V.R. Murty, Optimization of batch process parameters for Congo red color removal by *Neurospora crassa* live fungal biomass with wheat bran dual adsorbent using response surface methodology, Desal. Water Treat., 103 (2018) 84–101.

[17] A.A. Ichou, R. Benhiti, M. Abali, A. Dabagh, M. Chiban, M. Zerbet, G. Carja, F. Sinan, Adsorption of Pb(II) from aqueous solutions onto MgFeAl-CO$_3$ LDH: thermodynamic and kinetic studies, Desal. Water Treat., 178 (2020) 193–202.

[18] M. Yaghini, H. Faghihian, Novel magnetized carbon core-shell impregnated with lanthanum as an adsorbent for uptake of fluoride from aquatic systems, studied by response surface methodology, Desal. Water Treat., 179 (2020) 160–171.

[19] X.M. Wang, J.J. Feng, Z. Ma, J.Y. Li, D.M. Xu, X.J. Wang, Y.C. Sun, X.L. Gao, J. Gao, Application of response surface methodology for modeling and optimization of lead (Pb(II)) removal from seaweed extracts via electrodialysis, Desal. Water Treat., 179 (2020) 280–287.

[20] M.R. Sohrabi, S. Amiri, H.R.F. Masoumi, M. Moghri, Optimization of Direct yellow 12 dye removal by nanoscale zero-valent iron using response surface methodology, J. Ind. Eng. Chem., 20 (2014) 2535–2542.

[21] H.M.F Freundlich, Over the adsorption in solution, J. Phys. Chem., 57 (1906) 385–471.

[22] I. Langmuir, The adsorption of gases on plane surfaces of glass, mica and platinum, J. Am. Chem. Soc., 40 (1918) 1361–1403.

[23] M.A. Ahmad, N.K. Rahman, Equilibrium, kinetics and thermodynamic of Remazol Brilliant Orange 3R dye adsorption on coffee husk-based activated carbon, Chem. Eng. J., 170 (2011) 154–161.

[24] M.J. Temkin, V. Pyzhev, Kinetics of ammonia synthesis on promoted iron catalysts, Acta Physicochim. U.R.S.S., 12 (1940) 217–222.

[25] V.S. Munagapati, D.-S. Kim, Adsorption of anionic azo dye Congo red from aqueous solution by cationic modified orange peel powder, J. Mol. Liq., 220 (2016) 540–548.

[26] P. Vairavel, V.R. Murty, S. Nethaji, Removal of Congo red dye from aqueous solutions by adsorption onto a dual adsorbent (*Neurospora crassa* dead biomass and wheat bran): optimization,

isotherm, and kinetics studies, Desal. Water Treat., 68 (2017) 274–292.

[27] S. Lagergren, Zur theorie der sogenannten adsorption geloster stoffe, Kungliga svenska vetenskapsakademiens, Handlingar, 24 (1898) 1–39.

[28] Y.S. Ho, G. McKay, Pseudo-second-order model for sorption processes, Process Biochem., 34 (1999) 451–465.

[29] A.A. Oyekanmi, A.A.A. Latiff, Z. Daud, R.M.S.R. Mohamed, N.A.A. Aziz, N. Ismail, M. Rafatullah, A. Ahmad, K. Hossain, Adsorption of pollutants from palm oil mill effluent using natural adsorbents: optimization and isotherm studies, Desal. Water Treat., 169 (2019) 181–190.

[30] L. Largitte, R. Pasquier, A review of the kinetics adsorption models and their application to the adsorption of lead by an activated carbon, Chem. Eng. Res. Des., 109 (2016) 495–504.

[31] D. Pathania, A. Sharma, Z.-M. Siddiqi, Removal of Congo red dye from aqueous system using *Phoenix dactylifera* seeds, J. Mol. Liq., 219 (2016) 359–367.

[32] P.C. Jain, M. Jain, Engineering Chemistry (Chemistry of Engineering Materials), 9th ed., Dhanpat Rai & Sons Publishing Company Ltd., India, 1992.

[33] G.M. Yalvac, B. Bayrak, Use of natural and effective mandarin peel in elimination of Malachite green from the aqueous media: adsorption properties, kinetics and thermodynamics, Desal. Water Treat., 177 (2020) 176–185.

[34] V. Ponnusami, S. Vikram, S.N. Srivastava, Guava (*Psidium guajava*) leaf powder: novel adsorbent for removal of Methylene blue from aqueous solutions, J. Hazard. Mater., 152 (2008) 276–286.

[35] M.C. Somasekhara Reddy, Removal of direct dye from aqueous solutions with an adsorbent made from tamarind fruit shell, an agricultural solid waste, J. Sci. Ind. Res., 65 (2006) 443–446.

[36] M.K. Purkait, A. Maiti, S.D. Gupta, S. De, Removal of Congo red using activated carbon and its regeneration, J. Hazard. Mater., 145 (2007) 287–295.

[37] V. Vimonses, S.M. Lei, B. Jin, C.W.K. Chow, C. Saint, Kinetic study and equilibrium isotherm analysis of Congo red adsorption by clay materials, Chem. Eng. J., 148 (2009) 354–364.

[38] C. Namasivayam, D.J.S.E. Arasi, Removal of Congo red from wastewater by adsorption onto waste red mud, Chemosphere, 34 (1997) 401–417.

[39] C. Namasivayam, D. Kavitha, Removal of Congo red from water by adsorption onto activated carbon prepared from coir pith, an agricultural solid waste, Dyes Pigm., 54 (2002) 47–58.

[40] A. Tor, Y. Cengeloglu, Removal of Congo red from aqueous solution by adsorption onto acid activated red mud, J. Hazard. Mater., 138 (2006) 409–415.

[41] M.A. Zulfikar, H. Setiyanto, Rusnadi, L. Solakhudin, Rubber seeds (*Hevea brasiliensis*): an adsorbent for adsorption of Congo red from aqueous solution, Desal. Water Treat., 56 (2015) 2976–2987.

[42] I.D. Mall, V.C. Srivastava, N.K. Agarwal, I.M. Mishra, Removal of Congo red from aqueous solution by bagasse fly ash and activated carbon: kinetic study and equilibrium isotherm analyses, Chemosphere, 61 (2005) 492–501.

[43] S.-L. Chan, Y.P. Tan, A.H. Abdullah, S.-T. Ong, Equilibrium, kinetic and thermodynamic studies of a new potential biosorbent for the removal of Basic Blue 3 and Congo red dyes: pineapple (*Ananas comosus*) plant stem, J. Taiwan Inst. Chem. Eng., 61 (2016) 306–315.

[44] L. Wang, A.Q. Wang, Adsorption characteristics of Congo red onto the chitosan/montmorillonite nanocomposite, J. Hazard. Mater., 147 (2007) 979–985.

[45] G. Annadurai, R.-S. Juang, D.-J. Lee, Use of cellulose-based wastes for adsorption of dyes from aqueous solutions, J. Hazard. Mater., 92 (2002) 263–274.

[46] X.S. Wang, J.P. Chen, Biosorption of Congo red from aqueous solution using wheat bran and rice bran: batch studies, Sep. Sci. Technol., 44 (2009) 1452–1466.

[47] Y.Z. Fu, T. Viraraghavan, Removal of Congo red from an aqueous solution by fungus *Aspergillus niger*, Adv. Environ. Res., 7 (2002) 239–247.

[48] V.K. Gupta, D. Pathania, S. Agarwal, S. Sharma, Amputation of Congo red dye from waste water using microwave induced grafted *Luffa cylindrica* cellulosic fiber, Carbohydr. Polym., 111 (2014) 556–566.

[49] T. Taher, D. Rohendi, R. Mohadi, A. Lesbani, Congo red dye removal from aqueous solution by acid-activated bentonite from sarolangun: kinetic, equilibrium, and thermodynamic studies, Arabian J. Basic Appl. Sci., 26 (2019) 125–136

[50] C. Namasivayam, N. Muniasamy, K. Gayatri, M. Rani, K. Ranganathan, Removal of dyes from aqueous solutions by cellulosic waste orange peel, Bioresour. Technol., 57 (1996) 37–43.

[51] F.A. Pavan, S.L.P. Dias, E.C. Lima, E.V. Benvenutti, Removal of Congo red from aqueous solution by anilinepropylsilica xerogel, Dyes Pigm., 76 (2008) 64–69.

[52] H. Shayesteh, A. Rahbar-Kelishami, R. Norouzbeigi, Evaluation of natural and cationic surfactant modified pumice for Congo red removal in batch mode: kinetic, equilibrium, and thermodynamic studies, J. Mol. Liq., 221 (2016) 1–11.

[53] R.K. Gautam, V. Rawat, S. Banerjee, M.A. Sanroman, S. Soni, S.K. Singh, M.C. Chattopadhyaya, Synthesis of bimetallic Fe–Zn nanoparticles and its application towards adsorptive removal of carcinogenic dye Malachite green and Congo red in water, J. Mol. Liq., 212 (2015) 227–236.

[54] V.S. Mane, P.V. Vijay Babu, Kinetic and equilibrium studies on the removal of Congo red from aqueous solution using *Eucalyptus* wood (*Eucalyptus globulus*) saw dust, J. Taiwan Inst. Chem. Eng., 44 (2013) 81–88.

[55] U. Habiba, T.C. Joo, S.K.A. Shezan, R. Das, B.C. Ang, A.M. Afifi, Synthesis and characterization of chitosan/TiO_2 nanocomposite for the adsorption of Congo red, Desal. Water Treat., 164 (2019) 361–367.

[56] M. Abbas, M. Trari, Kinetic, equilibrium and thermodynamic study on the removal of Congo red from aqueous solutions by adsorption onto apricot stone, Process Saf. Environ. Prot., 98 (2015) 424–436.

[57] G.C. Panda, S.K. Das, A.K. Guha, Jute stick powder as a potential biomass for the removal of Congo red and rhodamine B from their aqueous solution, J. Hazard. Mater., 164 (2009) 374–379.

[58] Z.Y. Zhang, L. Moghaddam, I.M. O'Hara, W.O.S. Doherty, Congo red adsorption by ball-milled sugarcane bagasse, Chem. Eng. J., 178 (2011) 122–128.

[59] Z.H. Hu, H. Chen, F. Ji, S.J. Yuan, Removal of Congo red from aqueous solution by cattail root, J. Hazard. Mater., 173 (2010) 292–297.

[60] K.G. Bhattacharyya, S. Arunima, *Azadirachta indica* leaf powder as an effective biosorbent for dyes: a case study with aqueous Congo red solutions, J. Environ. Manage., 71 (2004) 217–229.

[61] S. Kumari, D. Mankotia, G.S. Chauhan, Crosslinked cellulose dialdehyde for Congo red removal from its aqueous solutions, J. Environ. Chem. Eng., 4 (2016) 1126–1136.

[62] K. Durairaj, P. Senthilkumar, V. Priya, P. Velmurugan, A.J. Kumar, Novel synthesis of *Chrysanthemum indicum* flower as an adsorbent for the removal of direct Congo red from aqueous solution, Desal. Water Treat., 113 (2018) 270–280.

[63] D. Garg, C.B. Majumder, S. Kumar, B. Sarkar, Removal of Direct blue-86 dye from aqueous solution using alginate encapsulated activated carbon (PnsAC-alginate) prepared from waste peanut shell, J. Environ. Chem. Eng., 7 (2019) 103365–103378.

[64] M.A. Salam, S.A. Kosa, N.A. Al-Nahdi, N.Y. Owija, Removal of Acid red dye from aqueous solution using zero-valent copper and zero-valent zinc nanoparticles, Desal. Water Treat., 141 (2019) 310–320.

[65] R. Sahraei, K. Hemmati, M. Ghaemy, Adsorptive removal of toxic metals and cationic dyes by magnetic adsorbent based on functionalized graphene oxide from water, RSC Adv., 76 (2016) 72487–72499.
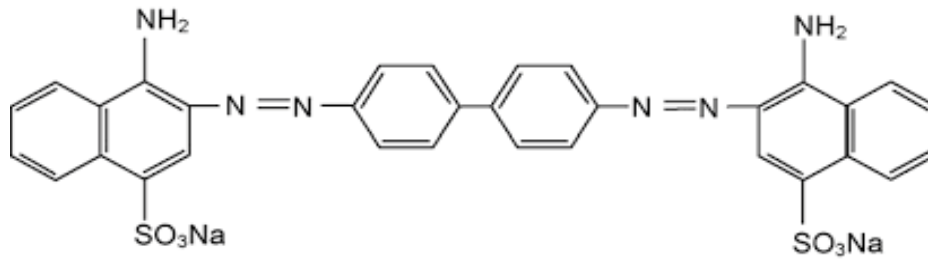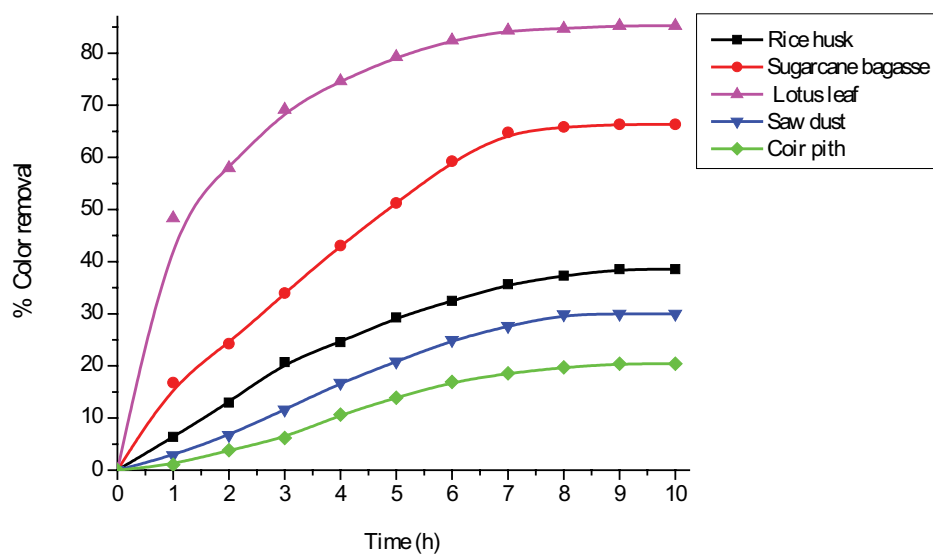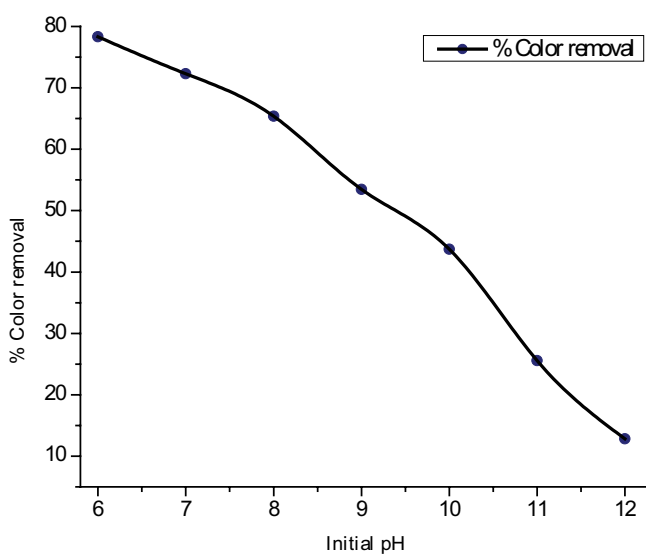
Supplementary information

Fig. S1. Chemical structure of Congo red dye.

Fig. S2. Selection of suitable agricultural by-product for the removal of CR dye. (Initial pH: 6; initial dye concentration: 200 mg L^{-1}; adsorbent dosage: 5 g L^{-1}; adsorbent particle size: <100 μm; agitation speed: 150 rpm; temperature: 303 K; contact time 10 h).

Fig. S3. Effect of initial pH on the removal of CR dye by LLP adsorbent. (Initial dye concentration: 250 mg L^{-1}; LLP adsorbent dosage: 5 g L^{-1}; LLP adsorbent particle size: 93.80 μm; agitation speed: 150 rpm; temperature: 303 K; contact time: 8 h).
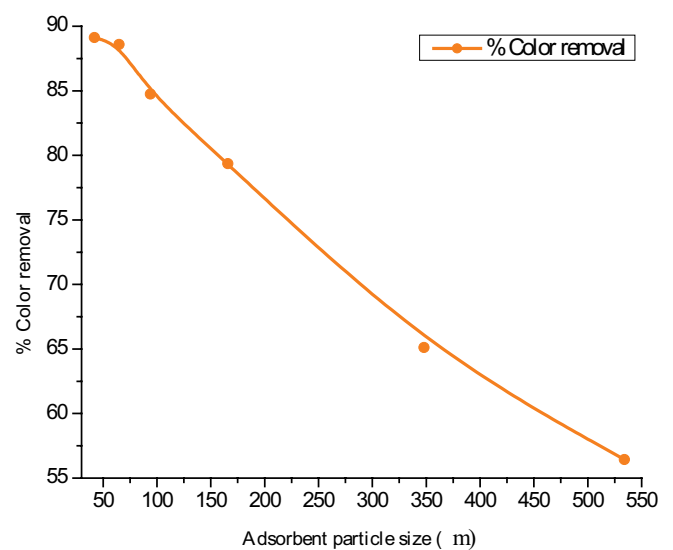
Fig. S4. Effect of LLP adsorbent particle size on CR dye adsorption. (Initial pH: 6; initial dye concentration: 250 mg L^{-1}; LLP adsorbent dosage: 6 g L^{-1}; agitation speed: 150 rpm; temperature: 303 K; contact time: 8 h).
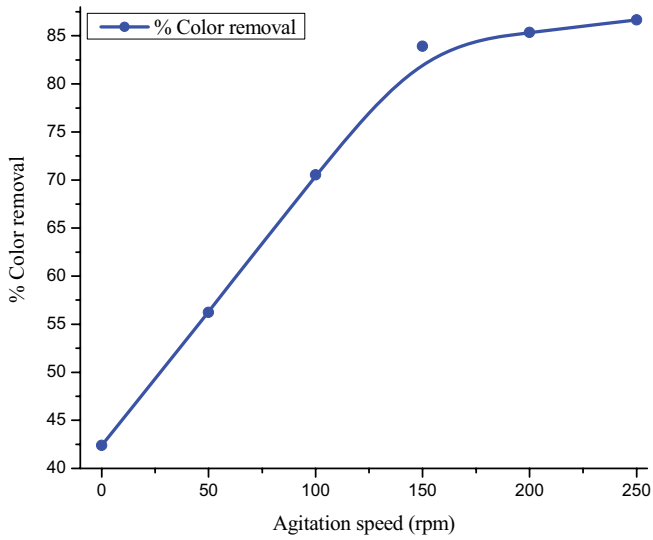
Fig. S5. Effect of agitation speed on the removal of CR dye by LLP adsorbent. (Initial pH: 6; initial dye concentration: 250 mg L^{-1}; LLP adsorbent dosage: 6 g L^{-1}; LLP adsorbent particle size: 93.80 μm; temperature: 303 K; contact time: 8 h).
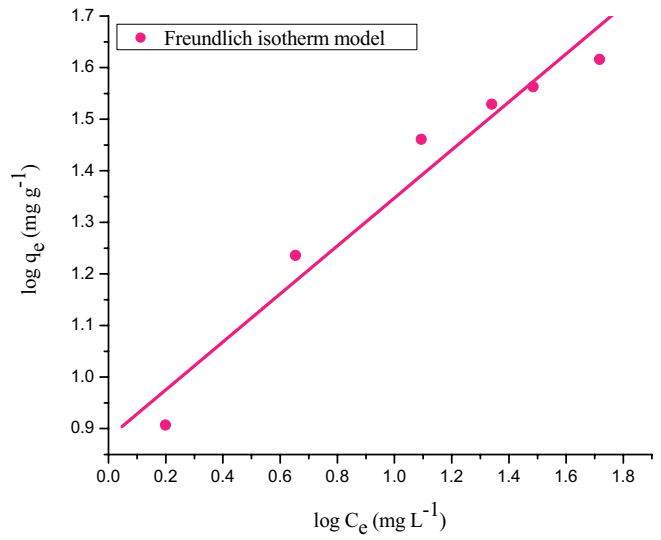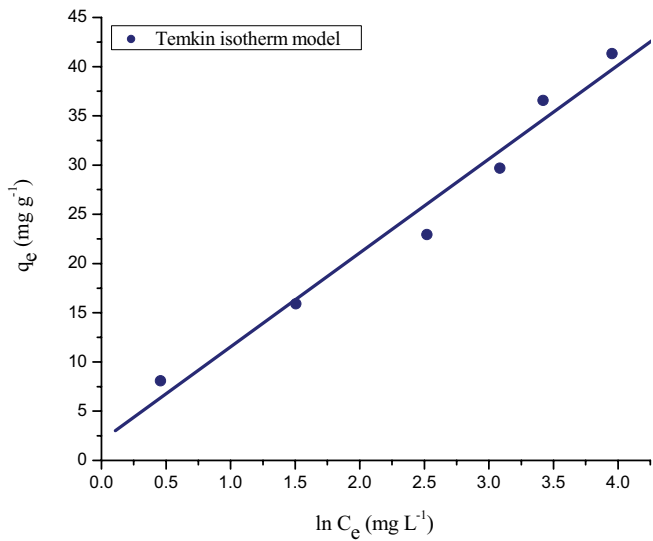

Fig. S6. Freundlich isotherm plot for adsorption of CR dye onto LLP adsorbent. (Initial pH: 6; initial dye concentration: 50–300 mg L^{-1}; LLP adsorbent dosage: 6 g L^{-1}; LLP adsorbent particle size: 93.80 μm; agitation speed: 150 rpm; temperature: 303 K; contact time: 24 h).

Fig. S7. Temkin isotherm plot for adsorption of CR dye onto LLP adsorbent. (Initial pH: 6; initial dye concentration: 50–300 mg L^{-1}; LLP adsorbent dosage: 6 g L^{-1}; adsorbent particle size: 93.80 μm; agitation speed: 150 rpm; temperature: 303 K; contact time: 24 h).
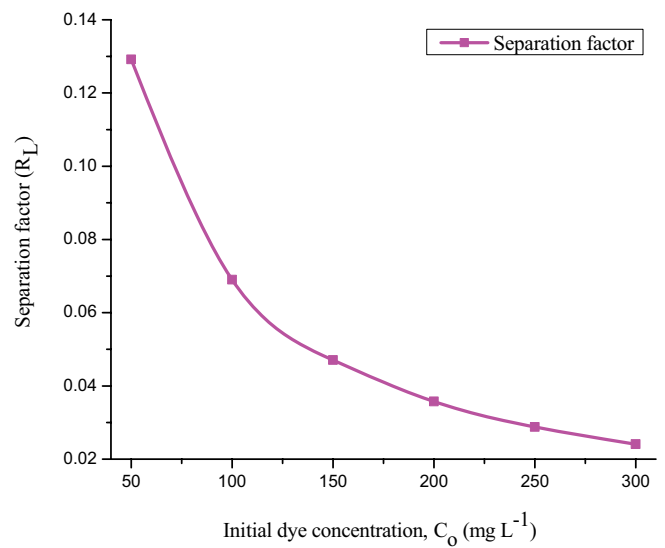

Fig. S8. Separation factor for adsorption of CR dye onto LLP adsorbent. (Initial pH: 6; initial dye concentration: 50–300 mg L^{-1}; LLP adsorbent dosage: 6 g L^{-1}; adsorbent particle size: 93.80 μm; agitation speed: 150 rpm; temperature: 303 K; contact time: 24 h).
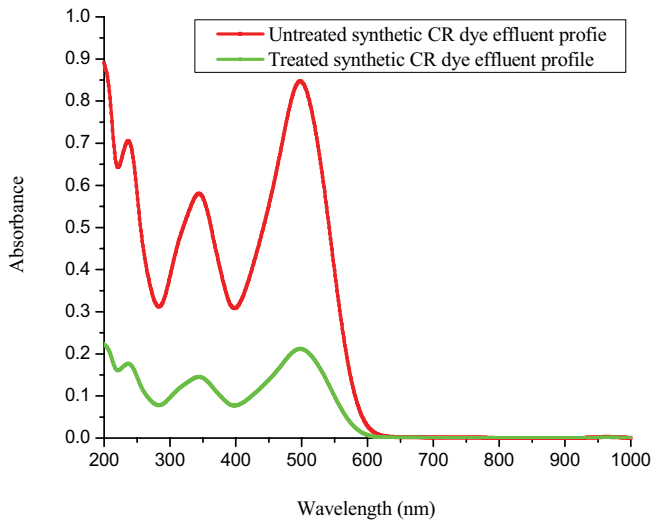
Fig. S9. Synthetic CR dye effluent decolorization profile was obtained in batch studies using LLP adsorbent as compared with untreated effluent. (Initial pH: 6; initial dye concentration: 100 mg L^{-1}; LLP adsorbent dosage: 6 g L^{-1}; LLP adsorbent particle size: 93.80 μm; agitation speed: 150 rpm; temperature: 303 K; contact time: 24 h).
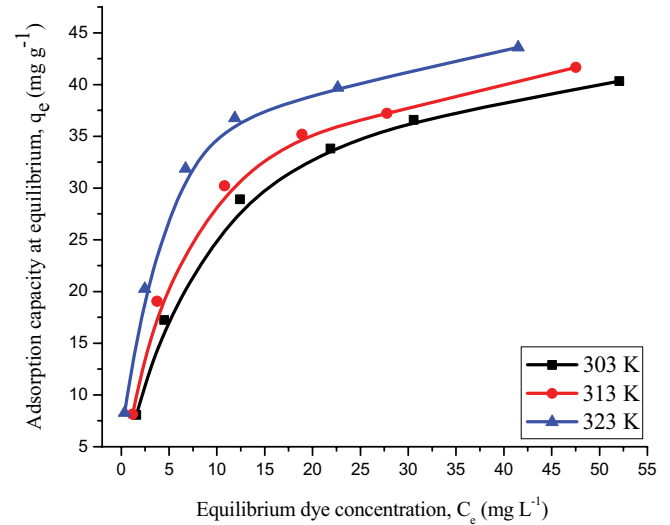

Fig. S10. Effect of temperature on adsorption of CR dye onto LLP adsorbent. (Initial pH: 6; initial dye concentration: 50–300 mg L^{-1}; LLP adsorbent dosage: 6 g L^{-1}; LLP adsorbent particle size: 93.80 μm; agitation speed: 150 rpm; contact time: 24 h).
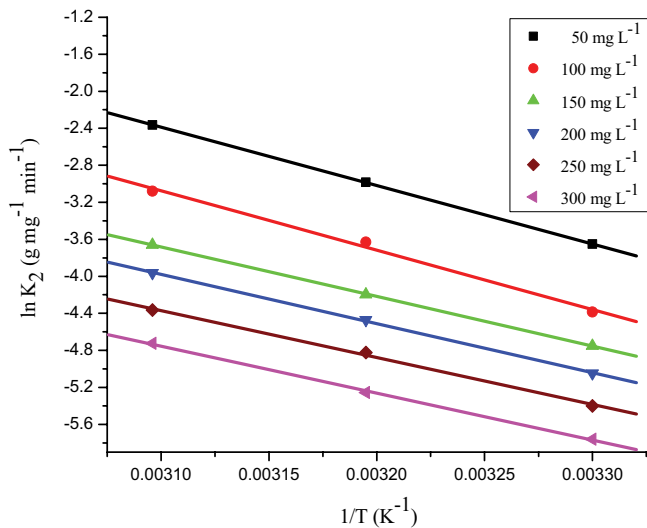

Fig. S11. Arrhenius plot for adsorption of CR dye onto LLP adsorbent. (Initial pH: 6; initial dye concentration: 50–300 mg L^{-1}; LLP adsorbent dosage: 6 g L^{-1}; LLP adsorbent particle size: 93.80 μm; agitation speed: 150 rpm; contact time: 24 h).
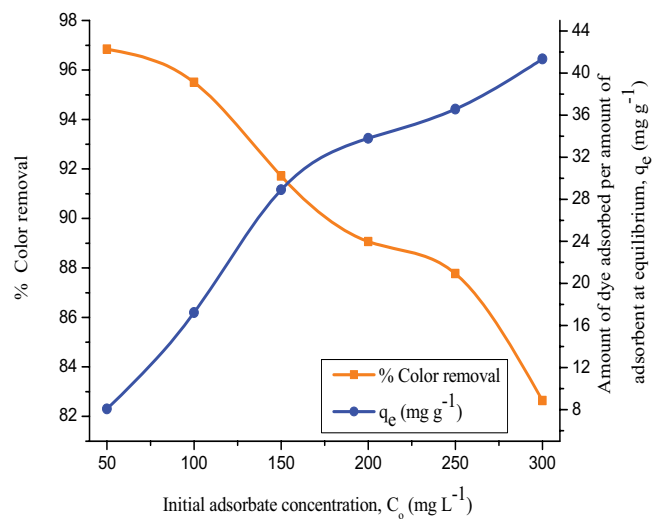

Fig. S12. Effect of initial dye concentration on the removal of CR dye by LLP adsorbent. (Initial pH: 6; LLP adsorbent dosage: 6 g L^{-1}; LLP adsorbent particle size: 93.80 μm; agitation speed: 150 rpm; temperature: 303 K; contact time: 24 h).
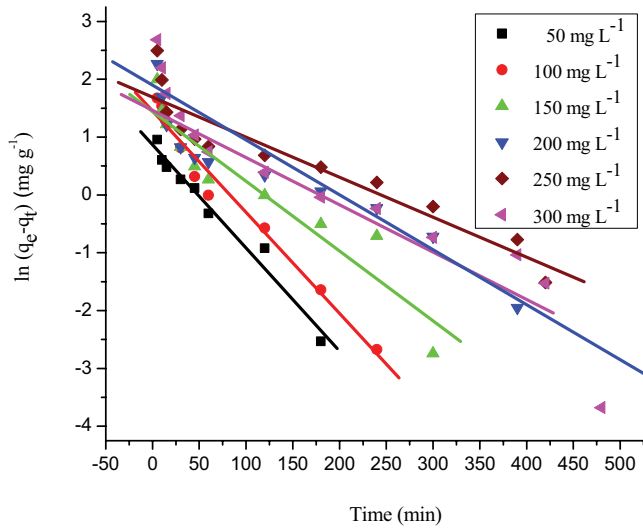
Fig. S13. Lagergren pseudo-first-order kinetic plot for adsorption of CR dye onto LLP adsorbent. (Initial pH: 6; initial dye concentration: 50–300 mg L⁻¹; LLP adsorbent dosage: 6 g L⁻¹; LLP adsorbent particle size: 93.80 μm; agitation speed: 150 rpm; temperature: 303 K; contact time: 24 h).
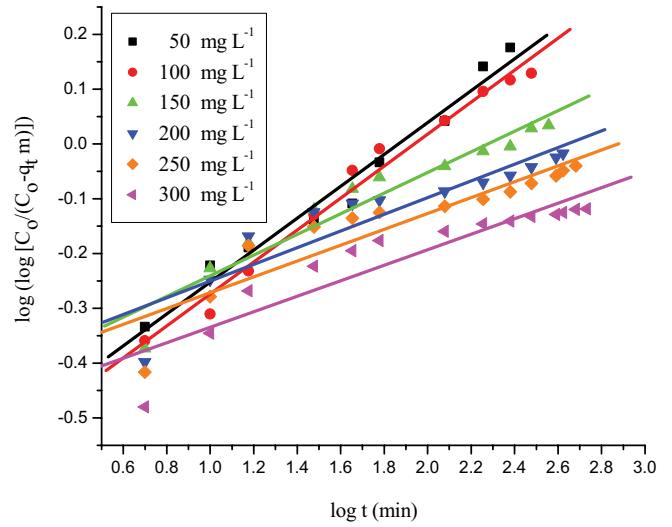
Fig. S14. Bangham plot for adsorption of CR dye onto LLP adsorbent. (Initial pH: 6; initial dye concentration: 50–300 mg L⁻¹; LLP adsorbent dosage: 6 g L⁻¹; LLP adsorbent particle size: 93.80 μm; agitation speed: 150 rpm; temperature: 303 K; contact time: 24 h).
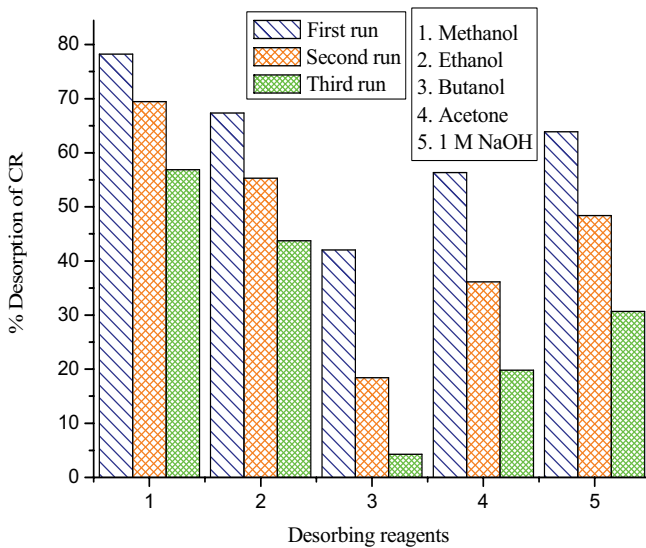
Fig. S15. Desorption efficiency of CR dye from LLP adsorbent in various runs. (Volume of desorbing reagent: 100 mL; shaking speed: 150 rpm; temperature: 303 K; contact time: 24 h).
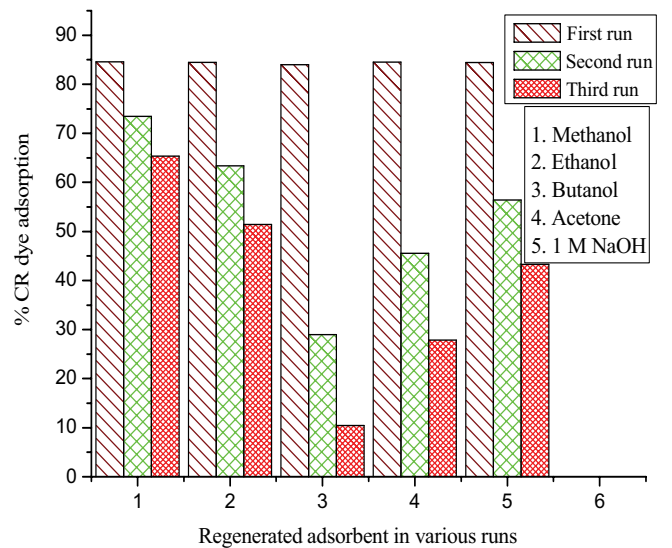
Fig. S16. Reusability of LLP adsorbent for the adsorption of CR dye in various runs. (Initial pH: 6; initial dye concentration: 200 mg L⁻¹; volume of dye solution: 100 mL; agitation speed: 150 rpm; temperature: 303 K; contact time: 24 h).

Table S1
Proximate analysis of LLP adsorbent

Parameters	Values (%)
Moisture content	10.34
Volatile matter	39.76
Ash content	7.38
Fixed carbon	42.52

Table S2
Chemical characterization of LLP adsorbent before and after adsorption

Process mode	Elements (weight %)		Elements (atom %)	
	Carbon	Oxygen	Carbon	Oxygen
Before adsorption	10.60	27.99	31.56	62.53
After adsorption	12.74	33.88	32.05	63.98

Table S3
ANOVA for % color removal of CR dye using LLP adsorbent from the data of CCD experiments

Term	Coefficient	SE of coefficient	$T_{statistics}$	DF	Seq. SS	Adj. SS	Adj. MS	$F_{statistics}$	Probability
Constant	84.0657	1.1622	72.333						0.000
Regression				14	2,552.21	2,552.21	182.30	19.28	0.000
Linear				4	1,734.85	1,734.85	433.71	45.87	0.000
X_1	–1.1233	0.6267	–1.790	1	30.29	30.29	30.29	3.20	0.092
X_2 (g L^{-1})	7.5325	0.6267	12.001	1	1,361.73	1,361.73	1,361.73	144.02	0.000
X_3 (μm)	–2.7217	0.6267	–4.336	1	177.78	177.78	177.78	18.80	0.001
X_4 (rpm)	2.6225	0.6267	4.178	1	165.06	165.06	165.06	17.46	0.001
Square				4	606.69	606.69	151.67	16.04	0.000
$X_1 \times X_1$	–0.5989	0.5750	–1.042	1	0.08	10.26	10.26	1.08	0.313
$X_2 \times X_2$ (g L^{-1})	–4.2464	0.5750	–7.385	1	453.71	515.64	515.64	54.54	0.000
$X_3 \times X_3$ (μm)	–0.9739	0.5750	–1.694	1	15.88	27.12	27.12	2.87	0.110
$X_4 \times X_4$ (rpm)	–2.1889	0.5750	–3.807	1	137.01	137.01	137.01	14.49	0.002
Interaction				6	210.68	210.68	35.11	3.71	0.017
$X_1 \times X_2$ (g L^{-1})	1.3138	0.7687	1.709	1	27.62	27.62	27.62	2.92	0.107
$X_1 \times X_3$ (μm)	1.2725	0.7687	1.655	1	25.91	25.91	25.91	2.74	0.117
$X_1 \times X_4$ (rpm)	0.5812	0.7687	0.756	1	5.41	5.41	5.41	0.57	0.461
X_2 (g L^{-1}) $\times X_3$ (μm)	–0.7887	0.7687	–1.026	1	9.95	9.95	9.95	1.05	0.320
X_2 (g L^{-1}) $\times X_4$ (rpm)	–1.9650	0.7687	–2.556	1	61.78	61.78	61.78	6.53	0.021
X_3 (μm) $\times X_4$ (rpm)	–2.2363	0.7687	–2.909	1	80.01	80.01	80.01	8.46	0.010
Residual error				16	151.28	151.28	9.45		
Lack-of-fit				10	151.21	151.21	15.12	1,323.09	0.000
Pure error				6	0.07	0.07	0.01		
Total				30	2,703.49				

Regression coefficient; R^2 = 94.40%; R^2 (Pred.) = 67.78%; R^2 (Adj.) = 89.51%; S = 3.07489; PRESS = 871.066.

Table S4
Activation energy for the adsorption of CR dye onto LLP adsorbent at various initial dye concentrations

Initial dye concentration, C_0 (mg L^{-1})	Activation energy, E_a (kJ mol^{-1})
50	52.495
100	53.358
150	44.526
200	44.136
250	42.188
300	42.219

Table S5
Kinetic parameters for the pore diffusion model at various initial CR dye concentrations

Initial dye concentration, C_0 (mg L^{-1})	Pore diffusion model		
	K_i (mg g^{-1} min$^{-1/2}$)	C	R^2
50	0.0916	6.561	0.9350
100	0.1104	14.036	0.9520
150	0.1208	20.614	0.9843
200	0.13303	26.871	0.9967
250	0.1654	32.844	0.9953
300	0.1460	38.075	0.9613

Table S6
Desorption studies for the removal of CR dye from LLP adsorbent in various runs

Sl. No	Desorbing reagent	% desorption of CR dye from LLP adsorbent		
		1st run	2nd run	3rd run
1	Methanol	78.214	69.438	56.852
2	Ethanol	67.358	55.267	43.724
3	Butanol	42.052	18.426	4.256
4	Acetone	56.327	36.134	19.820
5	1 M NaOH	63.899	48.372	30.658

Table S7
Reusability of LLP adsorbent for the adsorption of CR dye in various runs

Sl. No	Desorbing reagent	% adsorption of CR dye by regenerated LLP adsorbent		
		1st run	2nd run	3rd run
1	Methanol	84.575	73.485	65.364
2	Ethanol	84.454	63.394	51.456
3	Butanol	83.991	28.964	10.472
4	Acetone	84.513	45.573	27.854
5	1 M NaOH	84.394	56.432	43.265